AD-A153 302 CROSSED MOLECULAR BEAM STUDIES OF THE REACTIONS OF OXYGEN AND FLUORINE ATOMS(U) CALIFORNIA UNIV BERKELEY DEPT OF CHEMISTRY Y T LEE 20 MAR 85 N00014-83-K-0069 1/1

UNCLASSIFIED F/G 7/4 NL

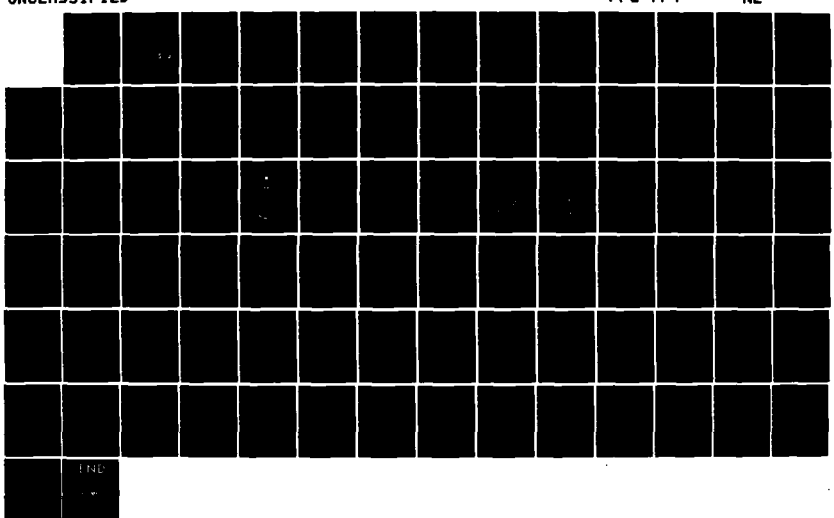

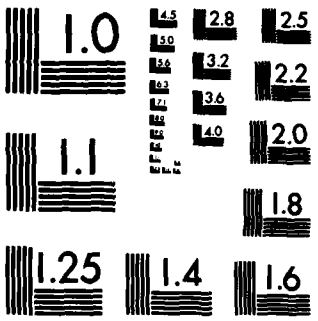

SECURITY CLASSIFICATION OF THIS PAGE (When Data Entered)

REPORT DOCUMENTATION PAGE

READ INSTRUCTIONS BEFORE COMPLETING FORM

1. REPORT NUMBER: NR 659-819/3/85	2. GOVT ACCESSION NO.
3. RECIPIENT'S CATALOG NUMBER	
4. TITLE (and Subtitle): CROSSED MOLECULAR BEAM STUDIES OF THE REACTIONS OF OXYGEN AND FLUORINE ATOMS	5. TYPE OF REPORT & PERIOD COVERED: ANNUAL REPORT 1/1/84-12/31/84
	6. PERFORMING ORG. REPORT NUMBER
7. AUTHOR(s): Yuan T. Lee	8. CONTRACT OR GRANT NUMBER(s): N00014-83-K-0069 NR 659-819
9. PERFORMING ORGANIZATION NAME AND ADDRESS: Professor Yuan T. Lee, Dept. of Chemistry, University of California, Berkeley, California 94720	10. PROGRAM ELEMENT, PROJECT, TASK AREA & WORK UNIT NUMBERS
11. CONTROLLING OFFICE NAME AND ADDRESS: Dr. Richard S. Miller, Office of Naval Research, Department of the Navy, Code 432P, 800 N. Quincy Street, Alrington, VA 22217	12. REPORT DATE: March 20, 1985
	13. NUMBER OF PAGES: 81
14. MONITORING AGENCY NAME & ADDRESS (if different from Controlling Office): Mr. Christal C. Grisham, Office of Naval Research Resident Representative, 197 Harmon Gym, University of Calif., Berkeley, CA 94720	15. SECURITY CLASS. (of this report): UNCLASSIFIED
	15a. DECLASSIFICATION/DOWNGRADING SCHEDULE

16. DISTRIBUTION STATEMENT (of this Report)

Unlimited

17. DISTRIBUTION STATEMENT (of the abstract entered in Block 20, if different from Report)

18. SUPPLEMENTARY NOTES

None

19. KEY WORDS (Continue on reverse side if necessary and identify by block number)

Photofragmenation translation spectrometer; molecular beams; unimolecular decay; photochemistry; photodissociation; rocket fuel; energetic materials.

20. ABSTRACT (Continue on reverse side if necessary and identify by block number)

This annual report describes the primary photodissociation of acetylene (C_2H_2) and bromoiodomethane (CH_2BrI) using a new molecular beam photofragmentation translational spectrometer.

(Continued on Reverse)

DD FORM 1 JAN 73 1473 EDITION OF 1 NOV 65 IS OBSOLETE
S/N 0102-LF-014-6601

SECURITY CLASSIFICATION OF THIS PAGE (When Data Entered)

20. Abstract (Continued)

The new third generation molecular beam photofragmentation translational spectrometer constructed during the past year is described in detail. This apparatus incorporates many new ideas and allows us to study some of the primary dissociation processes of polyatomic molecules which were not possible in the past.

In the photodissociation of C_2H_2 at 193 nm, it was found that the primary process is $C_2H_2 \xrightarrow{h\nu} C_2H + H$. A considerable amount of secondary photodissociation of C_2H, producing C_2 and H, was observed. The important information obtained includes the determination of the C-H bond dissociation energy in acetylene (~132 kcal/mole) and the vibrational excitation of the C_2H radical formed.

The dissociation of CH_2BrI at 248 and 193 nm is extremely interesting. The competition between C-I and C-Br bond rupture is the key question, but dissociation at 193 nm also produces IBr products. Secondary photodissociations of primary products were also found to be important.

These two systems are carried out partly for the purpose of evaluating the performance of the new molecular beam photofragmentation apparatus. The results clearly show that the performance of the apparatus is as good as our original expectation and that it should be capable of handling molecules with very low vapor pressures; studies of these molecules, such as the nitroamines, are planned.

Additional keywords: intramolecular decay; photochemistry; rocket fuels; energetic materials; polyatomic molecules; Naval research.

Annual Report on Contract Research Entitled

CROSSED MOLECULAR BEAM STUDY OF THE REACTIONS OF OXYGEN AND FLUORINE ATOMS

Prepared for the
Office of Naval Research
Department of the Navy

By
Yuan T. Lee
Professor of Chemistry
University of California
Berkeley, California 94720

Period Covered: January 1, 1984 to December 31, 1984

Technical Report No. NR 659-819/3/85

Contract Number N00014-83-K-0069

March 20, 1985

INTRODUCTION

Since three years ago the main theme of this research project has been the investigation of primary dissociation processes of polyatomic molecules.

Molecular beam photofragmentation translational spectroscopy has been shown to be an extremely powerful tool for the investigation of the dynamics and mechanisms of primary dissociation processes of polyatomic molecules. During the past year we have completed the construction of a new third generation molecular beam photofragmentation translational spectrometer which incorporates many new ideas resulting in a much higher sensitivity for handling molecules with lower vapor pressures.

In order to evaluate the performance of the new apparatus, a series of experiments were carried out. Two of the systems which were studied in greater detail are the photodissociation of C_2H_2 at 193 nm and the photodissociation of CH_2BrI at both 248 and 193 nm. In this report, the results obtained on these two systems will be described.

In the first section, in addition to the photodissociation of C_2H_2 at 193 nm, the new molecular beam apparatus will be described in great detail. The second part of the report will deal mainly with the photodissociation of CH_2BrI at 248 nm. The analysis of the results obtained at 193 nm is yet to be completed.

The systems to be investigated in the near future include the dissociation of CH_3NO_2, dimethylnitramine and a series of esters. In the investigation of CH_3NO_2, our main goal is to find out whethr the highly suspicious exit barrier of 10 kcal/mole suggested by Grant et al. is

real. In the dimethylnitramine, N-N bond rupture forming $(CH_3)_2N$ and NO_2 is expected to be the dominant channel, but whether there is also a concerted reaction channel forming HONO is not clear. In the series of systematic studies of esters, we will acquire new information on the dynamics and mechanisms of decomposition through cyclic transition states. Methyl acetate will be the most interesting one, since there is no single obvious low energy decay channel which is expected to be dominant.

I. THE PHOTODISSOCIATION OF C_2H_2 AT 193 NM

Acetylene is an important hydrocarbon in the area of combustion which has received a tremendous amount of attention in the past. The ultraviolet spectrum in the 200 nm range was analyzed and found to be due to absorption to a trans-bent ^1A_u excited state.[1,2] Electron energy loss spectroscopy was used to place the approximate energy of two low lying triplet states.[3] One aspect of this molecule which is still quite uncertain is the C-H bond dissociation energy. The lowest dissociative ionization threshold was measured to be 17.365 eV by Dibeler, Walker and McCulloh[4] (DWM) and more recently in a molecular beam by Ono and Ng (ON)[5] to be 16.79 eV. Combining the ionization potential (I.P.) of C_2H radical[6,7] with these thresholds, the C-H bond energy in neutral acetylene, $D_o(C-H)$ can be derived. But due to systematic deviations between experiments the uncertainty in the determination of $D_o(C-H)$ is still larger than 0.5 eV.

The advent and commercialization of excimer lasers (specifically ArF lasers at 193.3 nm) has allowed considerable advances in the study of the photochemistry of the ^1A_u absorption system. Irion and Kompa[8] have used an unfocused ArF laser to dissociate acetylene in a gas cell, analyzing the collisionally quenched, stable products with time-of-flight mass spectrometry. They concluded that C-H bond rupture was the primary unimolecular dissociation pathway

$$C_2H_2 \xrightarrow{193\ nm} C_2H + H \qquad (I)$$

McDonald, Baranovski, and Donnelly[9] and more recently Okabe, Cody, and Allen[10] have used a focused ArF laser (3×10^{18} photons/cm^2 pulse) to photolyze acetylene and observed two and three photon absorption processes to form C_2 and CH in excited electronic states which were observed by dispersed fluorescence spectroscopy. Again, using a strongly focused ArF laser, emission from electronically excited C atoms was observed by Miziolek, et al.[11]

In order to better understand the primary photodissociation processes involved and in an effort to determine D_o(C-H) in acetylene, we have recently performed molecular beam experiments designed to measure the translational energy release of fragments from the photolysis of acetylene at 193.3 nm under collision free conditions.

EXPERIMENTAL

The experiments were performed on a new molecular beam apparatus designed specifically for laser crossed molecular beam photodissociation studies. Some of the features of this machine are shown in Fig. 1. The instrument consists of three parts: a rotating molecular beam source, a fixed, ultra-high vacuum, mass-spectrometric detector, and a "main" interaction chamber.

A continuous molecular beam was formed by expanding 250 torr of a 15 percent mixture of acetylene in neon, which had been passed through a dry ice ethanol trap to remove acetone, through a 0.125 mm nozzle into the source region. The source region is pumped by two 6" diffusion pumps which do not move with the rotating source and maintain a pressure of 10^{-4} torr

when the beam is on. The beam is skimmed and a region of differential pumping intervenes between the source region and the main chamber. The differential region is normally at 10^{-5} torr pressure and is pumped by a 350 liter/sec turbo-molecular pump which rotates with the source. A pulsed laser beam, which comes out of the plane of the paper of Fig. 1, crosses the molecular beam at the point about which the source rotates, creating a pulse of dissociation products.

A small angular fraction of this pulse of products will travel through two regions of differential pumping, spreading as it goes due to the velocity distribution of the nascent products. The pulse is then ionized in a liquid nitrogen cooled chamber (typically 10^{-10} torr), by a Brink-type, electron-impact ionizer. Ions produced are directed through a quadrupole mass filter then to a Daly-type ion counter. The transient pulse arriving at various times or time-of-flight (TOF) spectrum is recorded on a 255 channel scaler operating as a pulse counter (minimum channel width is 1 μsec) which is triggered by the laser pulse. For higher time-of-flight resolution using narrower channel widths a digital delay was introduced on the trigger so that the transient pulse would be recorded over as many of the 255 channels as possible. The data acquisition is overseen and directed by a macro program running on a DEC LSI-11 lab computer. Typically one million pulses are collected at a repetition rate of 150 Hz for each time-of-flight spectrum.

The detector has precision machined slits in each of the walls through which the transient pulse passes, which define the detector's "viewing window." These are placed so that the detector views the entire intersection volume of the two beams at all angles. Any surfaces that are viewed by the

detector will be sources of background, because molecules scattered from these surfaces and moving toward the entrance slit will pass through all the defining slits and enter the ionizer directly. Consequently a closed cycle refrigerator was used to cool a copper collimation slit to 30°K. This lowers background originating from the main chamber by a factor of ten. Liquid nitrogen is supplied to the main chamber and cools large copper panels which serve as cryopumps. Undissociated acetylene strikes one of these panels. This is an effective beam catcher for condensible gases.

Data analysis consists of calculating the center-of-mass frame translational energy distribution function $P(E_T)$ from the observed laboratory frame TOF spectra. For the analysis of primary dissociation processes we use the "forward convolution" method. This means we guess at a trial $P(E_T)$ and calculate what our data should look like, taking into consideration several instrumental averaging factors including: beam velocity and angular dispersion, ionizer length, detector angular resolution and multichannel scaler channel width. We then alter the $P(E_T)$ until the calculated time-of-flight fits the data. For secondary dissociation we use a similar program which performs much more averaging. In this forward convolution program, the entire primary dissociation flux map in the three dimensional laboratory frame is calculated. This flux map is converted to number density and used to characterize the angular and velocity distributions of the "molecular beam" that the primary process gives rise to for the initial conditions of the secondary dissociation process. In a sense, looking at a secondary dissociation process is like looking at a primary process with a very poor molecular beam.

Experiments were done at two nozzle temperatures to observe the influence of unrelaxed bending vibrations in acetylene and also a neat beam of acetylene was used for low laser power experiments. Table I gives the beam characteristics.

The laser was a Lambda-Physik EMG 103 MSC Excimer laser and was run with ArF. Typially, 100 mJ/pulse at 150 Hz were obtained and focused to a 1 mm x 3 mm rectangular spot.

RESULTS

Laser photolysis of C_2H_2 gives signal at mass-to-charge ratios (m/e) of 25, 24, 13, and 12 amu. The signal at m/e=13 and 12 can be rationalized by electron-impact induced dissociative ionization of neutral products of masses 25 and 24. The time-of-flight spectra at 20 deg. for ion masses 25 and 24 are shown in Fig.2. The mass 25 signal can come only from C_2H radical produced in the photolysis process. C_2H^+ ions formed in the ionizer can easily fragment to C_2^+ and give rise to some of the signal at m/e=24. If C_2H were the only neutral product the m/e=25 and 24 spectra would be identical, apart from a very small difference in ion flight time. The m/e=24 spectrum shows a substantial amount of signal arriving at significantly shorter arrival times (higher translational energies) than the C_2H product and hence we conclude that C_2 is also formed in the collisionless photolysis. As will be shown in the next section from the laser power dependence of the dissociation signal, processes I and II which occur sequentially are responsible for the observed data.

$$C_2H_2 \xrightarrow{193\ nm} C_2H + H \qquad (I)$$

$$C_2H \xrightarrow{193\ nm} C_2 + H \qquad (II)$$

The strategy used to determine $D_o(C-H)$ in acetylene is as follows. When acetylene absorbs a photon at 193.3 nm it has 148 kcal/mol of energy at its disposal. We assume that the C_2H radical appearing with maximum translational energy corresponds to the ground state fragment. The validity of this assumption will be discussed below. The difference between the photon energy and the maximum translation energy release is $D_o(C-H)$. Although we can neglect any rotational energy of the parent acetylene which is mostly relaxed during the supersonic expansion, we cannot ignore unrelaxed vibrational energy in the two, doubly degenerate bending modes giving rise to products travelling faster than the true thermodynamic quantities would predict. The frequencies of these two vibrations are 611 cm^{-1} and 729 cm^{-1} which correspond to about 3kT at room temperature; we expect that these will not be cooled efficiently in the supersonic expansion. In principle, one could remove these "hot bands" by cooling the nozzle, but in practice it is easier to heat the nozzle to avoid cluster formation at low temperatures and identify the contributions from the "hot band" by observing a temperature dependent increase in the fastest products.

Time-of-Flight Spectra at 300°K Nozzle Temperature

Figure 3 shows the Newton diagram for the photolysis experiment for the 15 percent acetylene seeded in neon beam maintaining the nozzle temperature at 300°K. It shows the relation between the lab frame of reference and the center-of-mass frame of reference. The bold arrow represents the molecular beam velocity in the lab frame. The center-of-mass frame travels inertially along this vector. The circles which are drawn centered on the tip of this vector indicate various recoil speeds in the center-of-mass frame of reference for the C_2H fragment, that is, all lab velocities observed on a given circle are from the same center-of-mass recoil speed of the dissociating fragment. One can see that molecules with a large amount of internal excitation and hence low center-of-mass translational energies will not be scattered far from the beam. It is therefore necessary to look as close as 6° to the beam to see the most internally excited products. A further experimental consideration comes from the fact that the resolution of the measurement of the laboratory velocity is limited by the length of the ionizer compared to the total flight length, according to the following relationships.

$$\frac{\Delta V_{LAB}}{V_{LAB}} = \frac{\Delta t}{t} = \frac{\Delta L}{L} = \frac{1\ cm}{37\ cm} \simeq 0.03$$

where

ΔL = ionizer length (1 cm.)

L = flight length (37 cm.)

ΔV_{LAB} = lab velocity resolution element

V_{LAB} = lab velocity

Δt = arrival time resolution element

t = arrival time

It is also important to realize that at high lab velocities a certain velocity difference will be spread out in time to a lesser extent than at low lab velocities. Also, at large laboratory angles, in addition to the fact that the lab velocity for a given Newton circle is smaller, the separation between a pair of Newton circles in laboratory velocity space becomes larger. It is therefore always more favorable to look for features due to the differences in recoil velocities, such as different product vibrational states, at larger laboratory angles.

Figure 4 shows the data obtained at 28°, 20°, 17°, 10°, and 6° as well as the center-of-mass translational energy probability distribution, $P(E_T)$ used to fit the data. In Fig. 4, the circles are the data and the solid lines are the fit to the data. The structure that is being partially resolved is due to the internal state population distribution of the nascent C_2H radical. The peaks in the $P(E_T)$ have been labeled with arbitrary but "suggestive" symbols and correspond to the like labeled bumps and shoulders in the time-of-flight spectra.

Time-of-Flight Spectra of C_2H Fragment at 530°K Nozzle Temperature

In order to determine the contribution from "hot bands" the nozzle was heated to 530°K, roughly tripling (in comparison to the 300°K experiment) the number of parent acetylene molecules not in the ground state. The time-of-flight at 21° is shown in Fig. 5 along with the best fit $P(E_T)$. The only difference between the $P(E_T)$ at 530°K and the one at 300°K is the

approximate tripling of the peak marked H (suggestively "hot band") in the high temperature experiment. We therefore conclude that the maximum release of translational energy is slightly more than 16 kcal/mole, giving a D_o(C-H) of 132 kcal/mole.

Secondary Dissociation

Figure 6 shows the m/e=24 (C_2^+) time-of-flight and the best $P(E_T)$ which fits the data after removing the contribution from C_2H fragment. Although there is considerably less detail in the $P(E_T)$, the qualitative features are still apparent. The $P(E_T)$ appears to have two components. One is a sharp peak at about 10 kcal/mol and the other is a broad hump extending out to the maximum allowed translational energy.

DISCUSSION

Observed Collision Free Processes

The observation of laser induced m/e=25 signal at angles as large as 28°, and at lab velocities nearly twice that of the primary beam is conclusive evidence of C_2H radical being photochemically produced in the collision free environment of a molecular beam. The release of translational energy is consistent with a single photon being absorbed. Although this is hardly a surprising or controversial finding, it is a fairly important observation in that the presence of C_2H has always been inferred in past studies, while this is the first direct observation of the nascent C_2H radical in the gas phase.

There are two conceivable explanations to our m/e=24 data described by process III and IV.

$$C_2H_2 \xrightarrow{193\ nm} C_2H + H \xrightarrow{193\ nm} C_2 + H + H \qquad (III)$$

$$C_2H_2 \xrightarrow{2 \times 193\ nm} C_2 + H + H \qquad (IV)$$

Consideration of the $P(E_T)$ for the two photon dissociation allows us to eliminate a concerted mechanism for process IV. In a concerted three particle production, conservation of linear momentum would require the two hydrogen atoms to be emitted in exactly the same direction in order to produce C_2 at as large a laboratory-frame velocity as we are observing. Even in a cis-bent excited state this is difficult to imagine. If the two photon absorption of acetylene led to sequential loss of hydrogen atoms with time for the intermediate C_2H to rotate, it is possible that both hydrogen atoms could be emitted in the same direction. The sequential process III would also have no problem conforming to this constraint.

The most compelling evidence for eliminating process IV is the power dependent time-of-flight spectrum at m/e=25 shown in Fig. 7. This spectrum was taken with a neat acetylene beam for maximum signal. It has close to the same velocity as the neon seeded beam but the velocity distribution is nearly twice as broad. The circles show the time-of-flight spectrum taken at low power (5-10 mJ/pulse) while the solid line shows the spectrum at close to 100 mJ/pulse. If process IV were dominant we would expect only the magnitude and not the shape of the TOF to change. If process III predominates it is not at all unlikely that certain internal states of the

C_2H radical would have a higher absorption cross-section at 193.3 nm than others. This would give rise to a change in the shape of the m/e=25 TOF as a function of laser power, and that is exactly what has been observed in this experiment. It is evident that process III accounts for our observed data.

We do not see any obvious evidence for the molecular elimination channel V.

$$C_2H_2 \xrightarrow{193\ nm} C_2 + H_2 \qquad (V)$$

Sensitivity to the observation of this channel depends upon the amount of translational energy released in the reaction. The light H_2 products scatter in a much wider laboratory angular and velocity range, in addition, the smaller ionization cross section and shorter residence time in the ionizer make it much harder to detect than heavier fragments such as C_2H and C_2. We, must, therefore, confine our search to looking for C_2. In general if less translational energy is released, the experiment is more sensitive. In estimating a conservative upper limit to the importance of this channel we have assumed the worst case, that all of the available 4 kcal/mole appears as translation. This "masks" channel V so that it could appear very inconspicuously. Taking into consideration the relative ionization efficiences of C_2 and C_2H to give C_2^+, this leads to an upper limit for process V of 15 percent of process I. This is a very conservative estimate, since if the translational energy release is less (say 2 kcal/mole) the branching ratio is less than 2 percent.

It should be mentioned that we also did not observe CH product which is due to process VI

$$C_2H_2 \xrightarrow{2 \times 193\ nm} 2CH \qquad (VI)$$

which was a minor channel observed optically in ref. 8 and 9. McDonald et al. determined that VI is less than 1 percent of two-photon process III. This would almost certainly be beyond our limit of detection.

$\underline{P(E_T) \text{ for } C_2H_2 \xrightarrow{193\ nm} C_2H + H}$

In an experiment with infinite resolving power, because of the conservation of total energy the $P(E_T)$ would appear as a series of discrete peaks, one corresponding to each internal quantum state of the C_2H radical. Although it is not practical to resolve rotational quantum states of polyatomic molecules in the velocity measurements, structure due to vibrational state distributions can be observed in a favorable situation. In this experiment, we are able to see significant structure in the $P(E_T)$ due to the internal quantum state distribution of the C_2H. This is due primarily to the small amount of energy appearing as product rotation. Because C_2H_2 in the beam is rotationally cold, the rotational excitation of C_2H product will mainly come from the repulsive bond rupture in which orbital angular momentum of the departing fragments will be cancelled exactly by the rotational excitation of C_2H. But the creation of this pair of antiparallel angular momenta is constrained by the small mass of the departing hydrogen atom, which cannot carry away much angular momentum. In principle then, spectroscopic information is available through the $P(E_T)$. Assignment of the peaks, however, is anything but straightforward in this

case. If one assumes that our experiment resolves all the vibrational quantum states populated by the photolysis, then the widths of the peaks are due solely to rotational excitation. Table III shows the results of a simple angular momentum quantization calculation based on equation 2.

$$\mu v_{rel} b = J\hbar \qquad (2)$$

where μ = reduced mass ~1 g/mole

v_{rel} = relative velocity of departing fragments.

b = exit impact parameter (assumed to be 1 Å)

J = maximum rotational state available in C_2H.

The agreement with the observed width's of the peaks is striking and at once disturbing. This would imply assignment of peaks 0, 1, 2 and 3 to the ν_3 bending vibration of C_2H with a frequency of about 1100 cm^{-1}. Peak 1* could then easily be assigned to the v=0 level of the $C_2H(A^2\pi)$ state recently observed at 3692 cm^{-1},[12] or v=1 of the C-H stretch observed in a matrix at 3612 cm^{-1}.[13] However, ν_2 = 1100 cm^{-1} is a little hard to swallow compared to C_2H_2 bends at 600-700 cm^{-1}. In fact, there is no spectroscopic determination of the bending frequency in C_2H. Carrick et al.[10] estimate it from l-type doubling measurements to be between 390 and 475 cm^{-1} adding the caveat that vibronic coupling to the $A^2\pi$ state might increase the uncertainty of this estimate. Without further spectroscopic evidence, we would not recommend this interpretation of the $P(E_T)$.

A more likely explanation of the $P(E_T)$ would label the most closely spaced peaks, which are separated by about 550 cm^{-1} as sequential quanta of the bend. The inability to resolve all the peaks at higher translational energy can be explained in two ways. First, the inherent resolution of the experiment degrades as products release more and more translational energy, which can be seen from equation 1. Second, as shown in Table III, the rotational width of the vibrational peaks becomes larger than 550 cm^{-1} at energy releases greater than 8 kcal/mole. Even assuming the rotational width to remain small, Fig. 8 shows that a highly structured $P(E_T)$ does not affect the fit to the data, which simply restates the fact that the resolution is degrading for the faster products. If, in addition to this, more than one vibrational mode in C_2H is excited by the photolysis the situation would be more complicated. This is indeed not unreasonable. Simple Frank-Condon comparison between the ^1A_u state of C_2H_2 and $^2\Sigma$ state of C_2H would predict bending and C-C stretching to be excited. The bend is excited because it is going from a bent to a linear state and the C-C stretch is excited because the C-C bond order increases upon going from ^1A_u C_2H_2 to $^2\Sigma$ C_2H.

The general shape of the $P(E_T)$ is intriguing. It appears that the translational energy peaks well away from zero. This would argue against internal conversion playing an important role in the radiationless processes which lead to products. For the analagous formaldehyde system,[14] excitation at 20 kcal/mole above the S_1 origin led to radical formation in the ground electronic state of HCO. However, the $P(E_T)$ looked like a typical bond fission process observed in infrared multiphoton-dissociation

experiments which occur along S_0 of the parent, that is the translational energy peaked at zero. This raises two questions. Is the apparent peak away from zero due to secondary dissociation burning away preferentially the most internally excited C_2H molecule? If not, is there an exit channel barrier or curve crossing affecting the dynamics? We believe that even if the secondary process is altering the exact shape of the $P(E_T)$ the qualitative features would not change as the laser power approached zero.

$P(E_T)$ for $C_2H \xrightarrow{193\ nm} C_2 + H$

In fluorescence emission work,[8,9] the C_2 Phillips band has been observed. This is a result of the $^1\pi_u$ state which is formed with 25 kcal/mole excess energy. In the $P(E_T)$ shown in Fig. 6 it is easy to see a sharp peak at around (10 kcal/mole), which we attribute to $^1\pi_u$ of C_2. This sharp peak has underlying it a broad hump originating from two low lying electronic states of C_2 ($^1\Sigma_g$ or $^3\Sigma_u$ or both). We see no evidence of three photon processes at our laser powers (10^{18} photons/cm^2 pulse), nor any 2-photon processes which would give $C_2 + H_2$ with a great deal more release of translational energy. In summary, Table IV lists our observed channels compared to those that have been hypothesized.

The C-H Bond Energy in Acetylene

In previous experiments, the C-H bond energy was determined indirectly by measuring the dissociative ionization threshold for acetylene and the Ionization Potential (I.P.) for the C_2H radical, that is processes VII and VIII respectively.

(VII) $C_2H_2 \longrightarrow C_2H^+ + H + e^-$ E_{VII}

(VIII) $C_2H \longrightarrow C_2H^+ + e^-$ E_{VIII}

Dibeler, Walker and McCulloh (DWM) measured E_{VII} very carefully, looking at the temperature dependence of hotbands near threshold to get a value of 17.37 ± 0.01 eV. Recently, Ono and Ng[5] (ON) have disputed this value on the basis of a very sensitive molecular beam photoionization threshold measurement. ON claim the threshold to be 16.79 ± 0.03 eV. This, however is almost certainly due to the ion pair channel as shown recently by Page et al.[15]

The I.P. of C_2H was measured directly by Wyatt and Stafford[4] (WS) using electron impact threshold ionization and they obtain a value of 11.6 ± 0.5 eV. In two much more precise experiments, Okabe and Dibeler (OD) and Miller and Berkowitz (MB) have obtained 11.96 ± 0.05 eV and 11.51 ± 0.05 eV respectively. Their experiments are conceptually shown in Fig. 9 where the numbers with asterisks are the measured values. Table IV shows all possible values of the C-H bond energy by combining in all possible ways the various experiments.

As can be seen, this work substantiates the values reported by DWM and MB. All the values calculated using the results of O.N. are far too low (by about the electron affinity of H).

As mentioned previously, our $D_0(CH)$ determination rests upon the assumption that it is possible for all available energy to appear as translation in some of the products. We expect vibronic coupling to be

strong enough to break the electronically adiabatic correlation rules for two reasons. First, there is 27 kcal/mole of vibrational energy above the ^1A_u origin in the parent excited state acetylene. In the analagous system of formaldehyde, the S_1 state had no difficulty in undergoing internal conversion and subsequent radical formation with only 20 kcal/mole vibrational energy. The $P(E_T)$ however peaked at very low translational energies, unlike the $P(E_T)$ for C_2H_2.

There are less than twenty non-rotational internal states energetically accessible in the C_2H product. Statistically we expect there to be a significant population in each state. In other words, we do not expect to see a $P(E_T)$ which tails away very slowly to zero on the high energy end. We expect instead a rather sharp rise from zero. We believe, because of the small number of degrees of freedom and the excellent signal/noise in our data, that 16.25 ± 2 kcal/mole is an accurate determination of the maximum release in translational energy and hence, the bond energy in acetylene is found to be 132 kcal/mole.

CONCLUSIONS

We have measured the translational energy distribution for acetylene photodissociation at 193.3 nm. The primary processes are

$$C_2H_2 \xrightarrow{193\ nm} C_2H + H \qquad \text{I}$$

$$C_2H \xrightarrow{193\ nm} C_2 + H \qquad \text{II}$$

Process II is important even at fluences below 10^{18} photons/cm^2 pulse. The translational energy distribution for I shows up to 16.25 kcal/mole translational energy release implying a D_0(C-H) of 132 kcal/mole. This is the first time that this important thermodynamic quantity has been measured in a single experiment. The vibrational structure of C_2H is partially resolved and we conclude that the bending frequency in C_2H is near 550 cm^{-1}. The data in our experiment could be analyzed more meaningfully if the spectroscopic data on C_2H were more complete. The translational energy distribution for II is consistent with fluorescence work showing population of $C_2(^1\pi_u, {}^1\Sigma_g)$. Future work in our group will include a detailed power dependence study in an effort to further assign the peaks in Fig. 4, polarization dependent experiments and development of a C_2H radical source via pulsed quartz nozzle, pulsed laser expansion.

REFERENCES

1. C. K. Ingold, G. W. King, J. Chem. Soc. 2702 (1953).

2. K. Keith Innes, J. Chem. Phys. 22, 863 (1954).

3. S. Trajmar, J. K. Rice, P. S. P. Wei, A. Kuppermann, Chem. Phys. Lett. 1, 703 (1968).

4. Vernon H. Dibeler, James A. Walker, K. E. McCulloh, J. Chem. Phys. 59, 2264 (1973).

5. Y. Ono, C. Y. Ng, J. Chem. Phys. 74,. 6985 (1981).

6. H. Okabe, V. H. Dibeler, J. Chem. Phys. 59, 2430 (1973).

7. J. Berkowitz, Photoabsorption, Photoionization, and Photoelectron Spectroscopy, Academic Press, New York, 1979, pp. 285-290.

8. M. P. Irion, K. L. Kompa, Appl. Phys. B27, 183 (1982).

9. J. R. McDonald, A. P. Baranovski, V. M. Donnelly, Chem. Phys. 33, 161 (1978).

10. H. Okabe, R. J. Cody, J. E. Allen Jr., XVIth Informal Conference on Photochemistry, Harvard University (1984).

11. Private communication.

12. P. G. Carrick, A. J. Merer, R. F. Curl Jr., J. Chem. Phys. 78, 3652 (1983).

13. Marylin E. Jacox, Chem. Phys. 7, 424 (1975).

14. Pauline Ho, Douglas J. Bamford, Richard J. Buss, Yuan T. Lee, C. Bradley Moore, J. Chem. Phys. 76, 3630 (1982).

15. R. Page, A. Kung, R. Larkin, to be published.

Table I

Expansion Conditions	$\Delta V/V$	Most Probable Velocity	ΔE_T^{LAB}
Seeded 300°K	12	7.9×10^4 cm/s	1 kcal/mole
Seeded 300°K	12	10.8×10^4 cm/s	1 kcal/mole
Neat 300°K	25	8.36×10^4 cm/s	2 kcal/mole

Table II

Peak Label	Translational Energy	J	E_{rot}^{max}
0	14 kcal/mole	18	3 kcal/mole
1	10 kcal/mole	15	2 kcal/mole
2	7.5 kcal/mole	13	1.5 kcal/mole
1*	6 kcal/mole	12	1.3 kcal/mole
3	4 kcal/mole	10	0.9 kcal/mole

Table III

CHANNEL	OBSERVED
$C_2H_2(^1\Sigma_g^+) \xrightarrow{193\ nm} C_2H(^2\Sigma, ^2\Pi) + H$	Yes
$C_2H \xrightarrow{193\ nm} C_2(^1\Sigma_g^+) + H$	Yes
$C_2H \xrightarrow{193\ nm} C_2(^1\Pi_u) + H$	Yes
$C_2H_2(^1\Sigma_g^+) \xrightarrow{2 \times 193\ nm} C_2 + H_2$	No
$C_2H_2(^1\Sigma_g^+) \xrightarrow{193\ nm} C_2 + H_2$	No

Table IV

Combination	C-H Bond Energy
D.W.M. a W.S.	133 kcal/mole ± 1.2 kcal/mole
D.W.M. a M.B.	135 kcal/mole ± 1.4 kcal/mole
D.W.M. a O.D.	125 kcal/mole ± 1.4 kcal/mole
O.N. a W.S.	116 kcal/mole ± 1.2 kcal/mole
O.N. a M.B.	118 kcal/mole ± 1.8 kcal/mole
O.N. a O.D.	107 kcal/mole ± 1.8 kcal/mole
This work	132 kcal/mole

FIGURE CAPTIONS

Fig. 1. The new molecular beam photodissociation machine. (1) Gas feed line to nozzle. (2) Liquid helium cooled collimation slit. (3) Interaction zone. (4) Liquid nitrogen cooled beam catcher. (5) Liquid nitrogen cooled copper panels. (6) Removeable time-of-flight wheel, for measuring primary beam velocity distribution. (7) Brink-type ionizer. (8) Quadrupole mass filter. (9) Exit ion optics. (10) Ion target (Daly detector). (11) Scintillator (Daly detector). (12) Photomultiplier tube (Daly detector). (14) Magnetically suspended turbomolecular pump. (15) Conventional turbomolecular pumps.

Fig. 2. Mass 25 and 24 time of flight spectra. The circles are m/e=24, the crosses are m/e=25. Signal was observed at a source angle of 20°.

Fig. 3. Newton diagram for seeded beam at 300°K. The angles shown are where data was taken. The circles represent the indicated amount of translational energy release for process I.

Fig. 4. Data observed and best fit $P(E_T)$. The peaks labeled in the $P(E_T)$ correspond to the features in the TOF data with the same labels. The circles are the data and the solid lines are the best fit from the $P(E_T)$.

Fig. 5. Data and $P(E_T)$ for the experiment at 21° with a seeded beam at 530°K. Circles are data while the solid line the fit to the data.

Fig. 6. Data at m/e=24 and best fit $P(E_T)$ for secondary dissociation process. The circles are data, the dashed line is secondary dissociation and the dotted line is the primary dissociation.

Fig. 7. Power dependent time-of-flight spectra. The circles are at 5 mJ/pulse laser power, while the solid line is data taken at 100 mJ/pulse.

Fig. 8. $P(E_T)$ assuming a bending vibration progression of about 500 cm^{-1} and the resulting fit to the data.

Fig. 9. Ionization potential determination of Okabe and Dibeler and of Miller and Berkowitz. Numbers with asterisks are measured thresholds. Numbers without asterisks are known values.

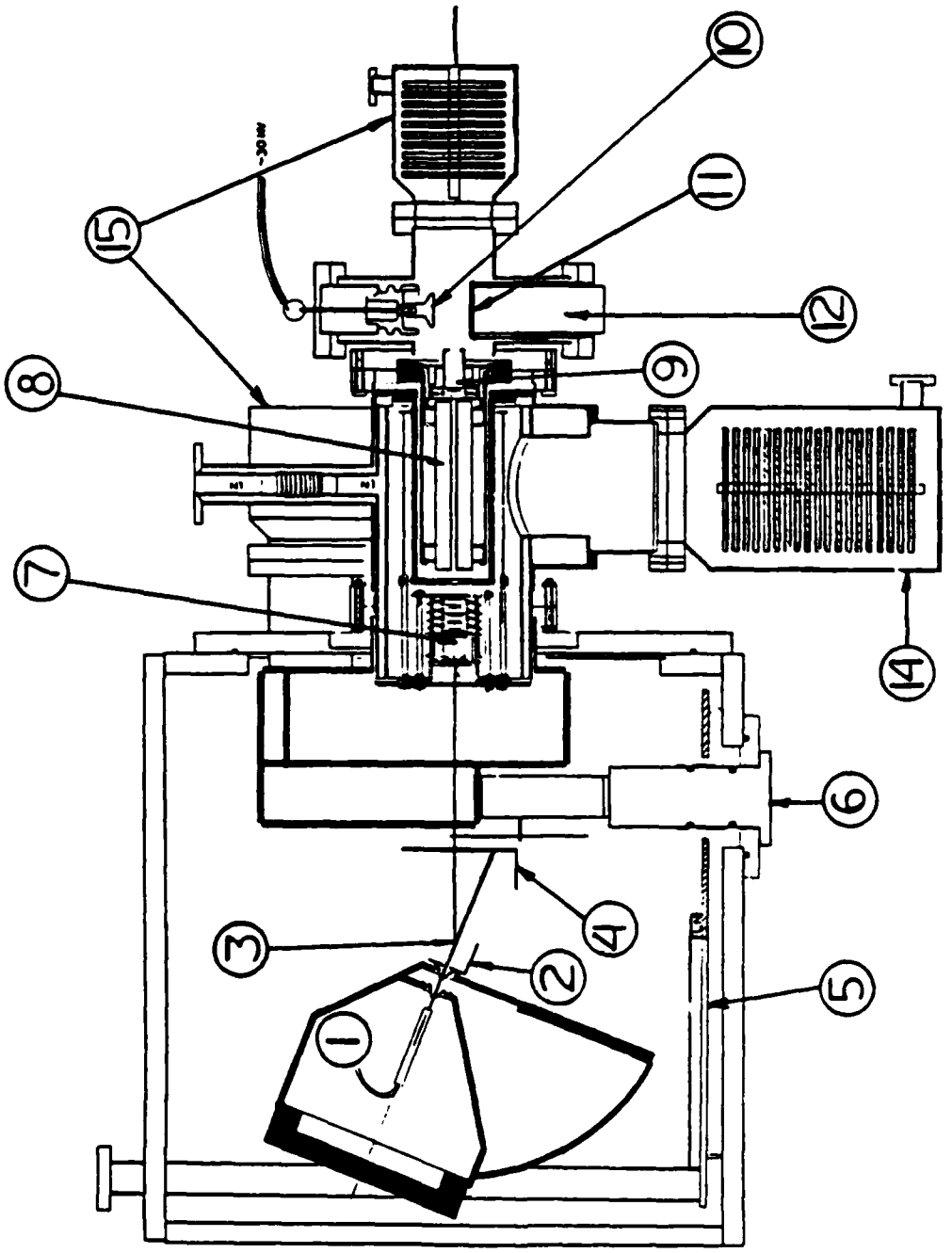

XBL 849-4028

Fig. 1

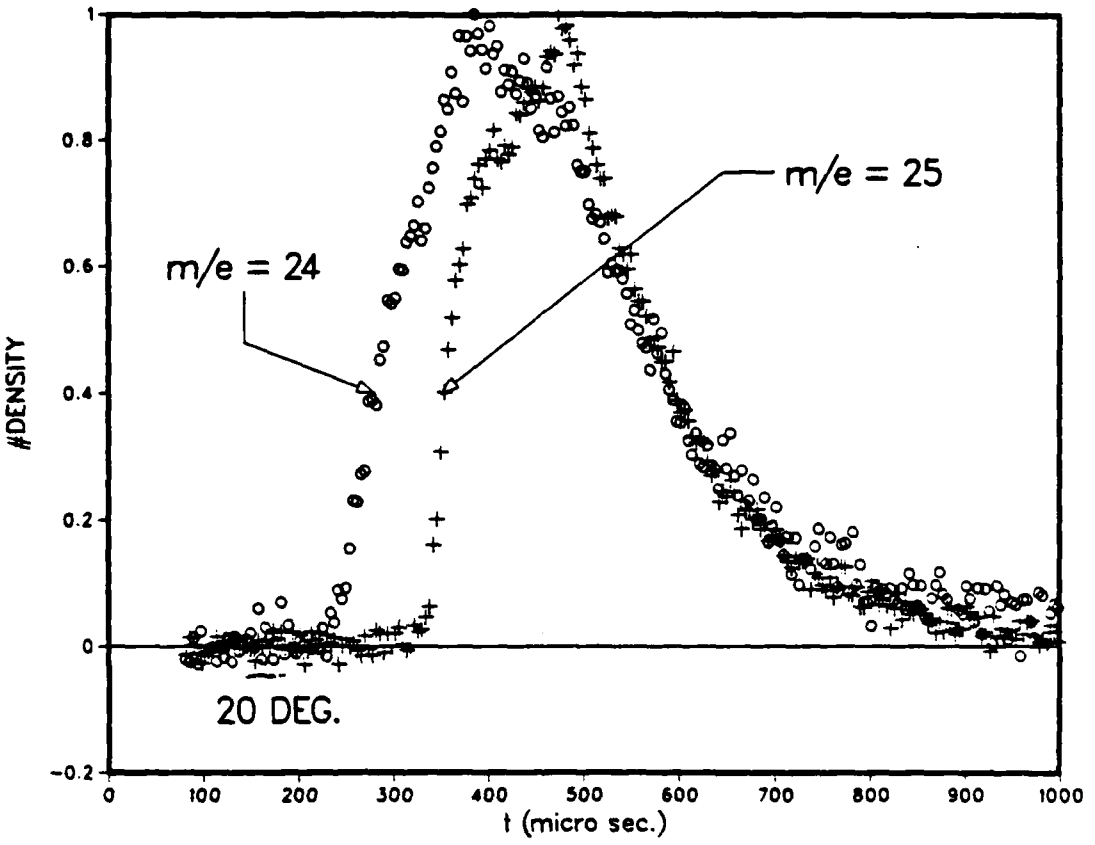

XBL 852-1156

Fig. 2.

NEWTON DIAGRAM FOR 300 DEG. KELVIN

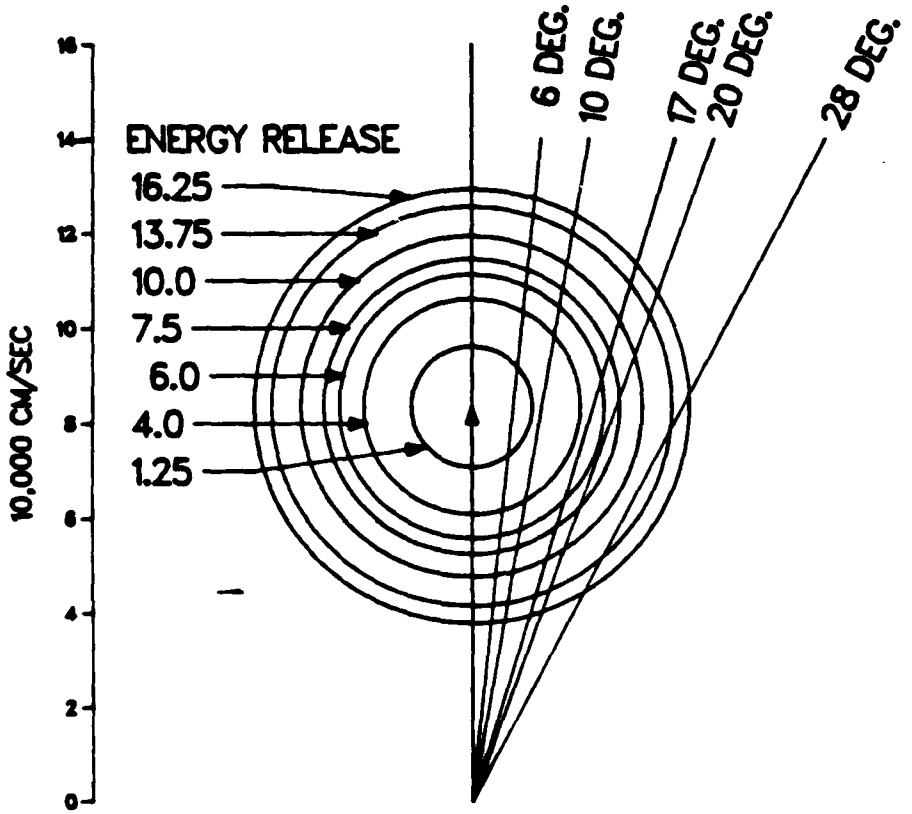

XBL 852-1158

Fig. 3.

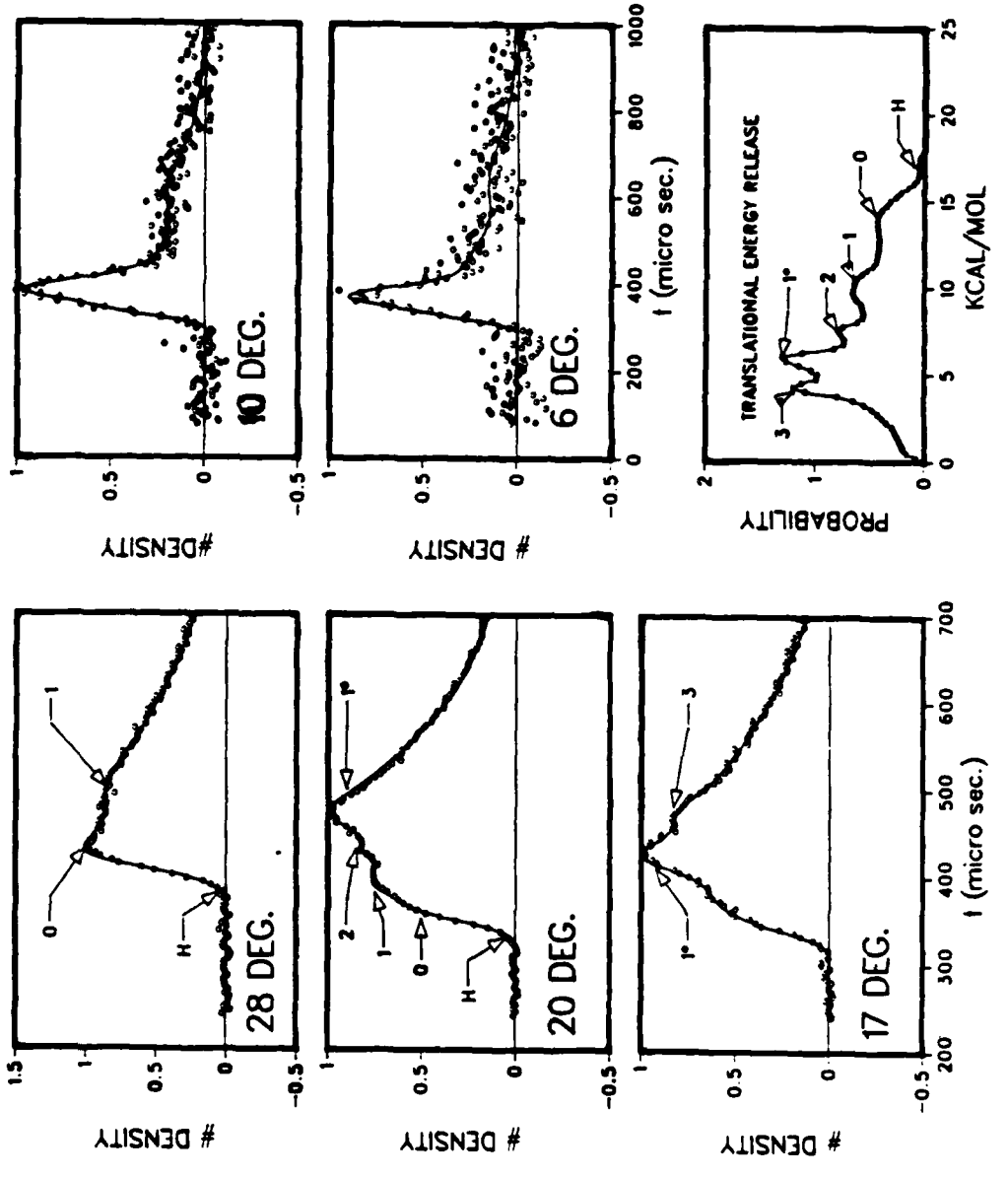

XBL 852-1161

Fig. 4.

530 DEG. KELVIN EXPERIMENT

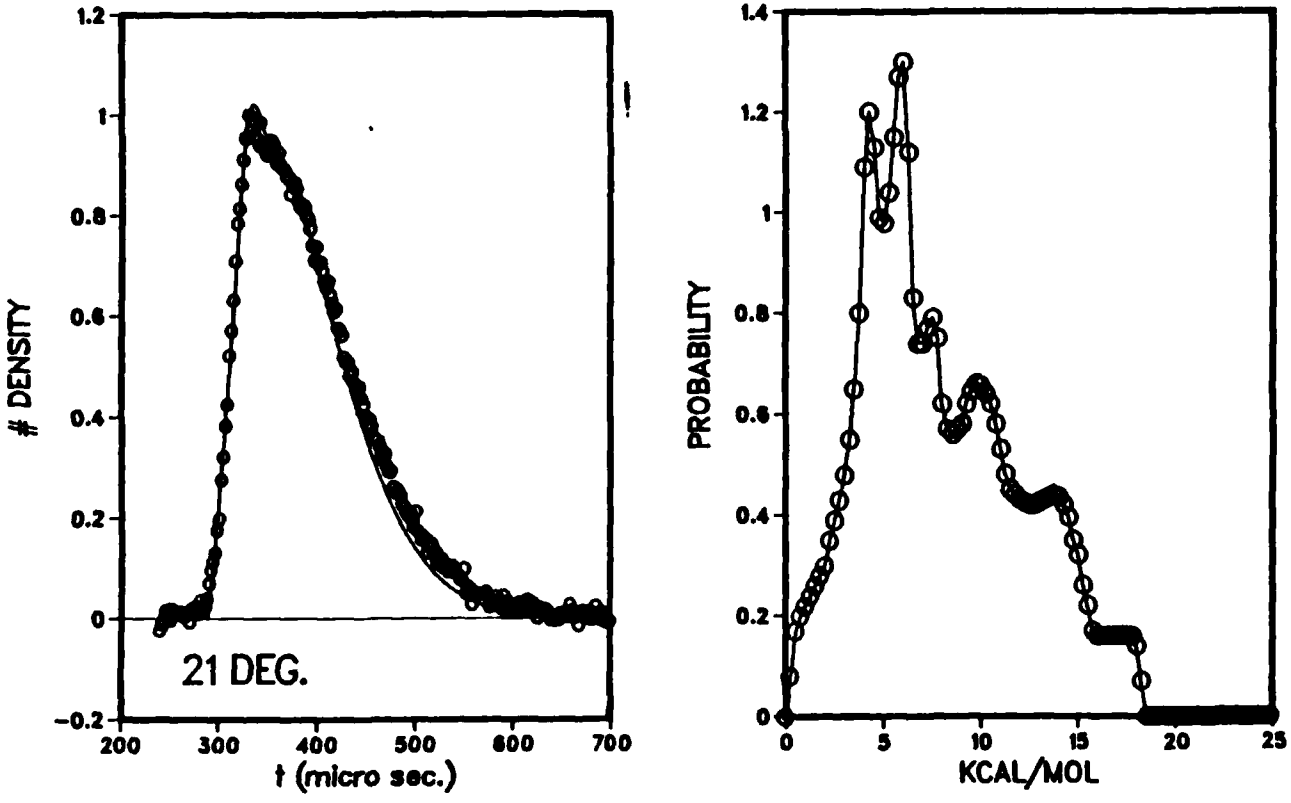

Fig. 5.

XBL 852-1160

SECONDARY DISSOCIATION

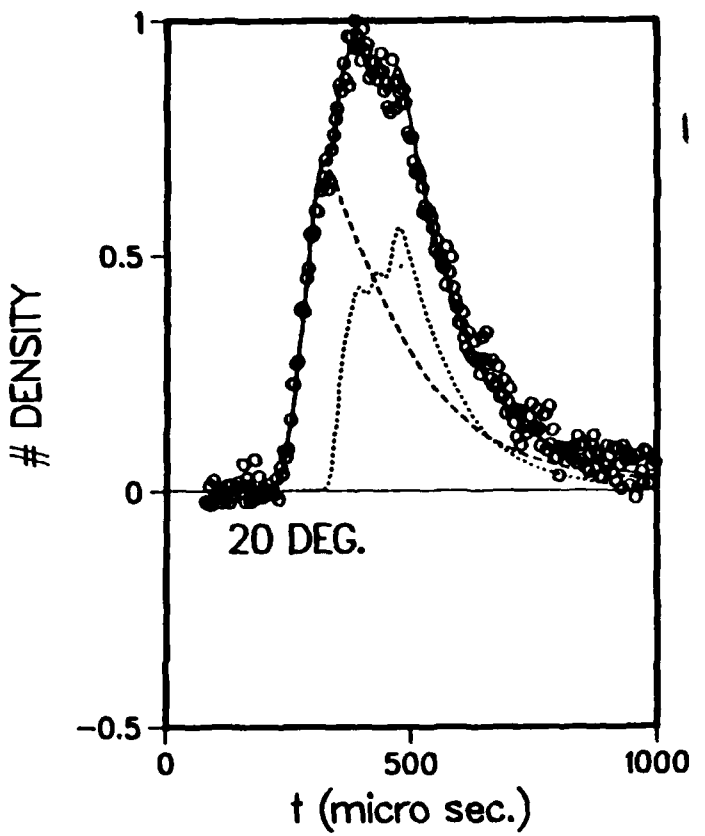

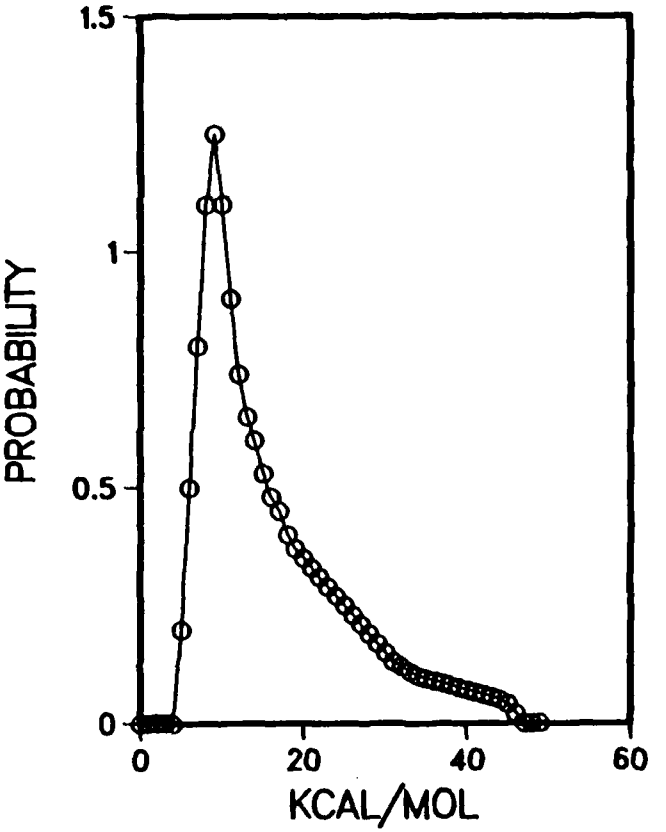

Fig. 6.

XBL 852-1159

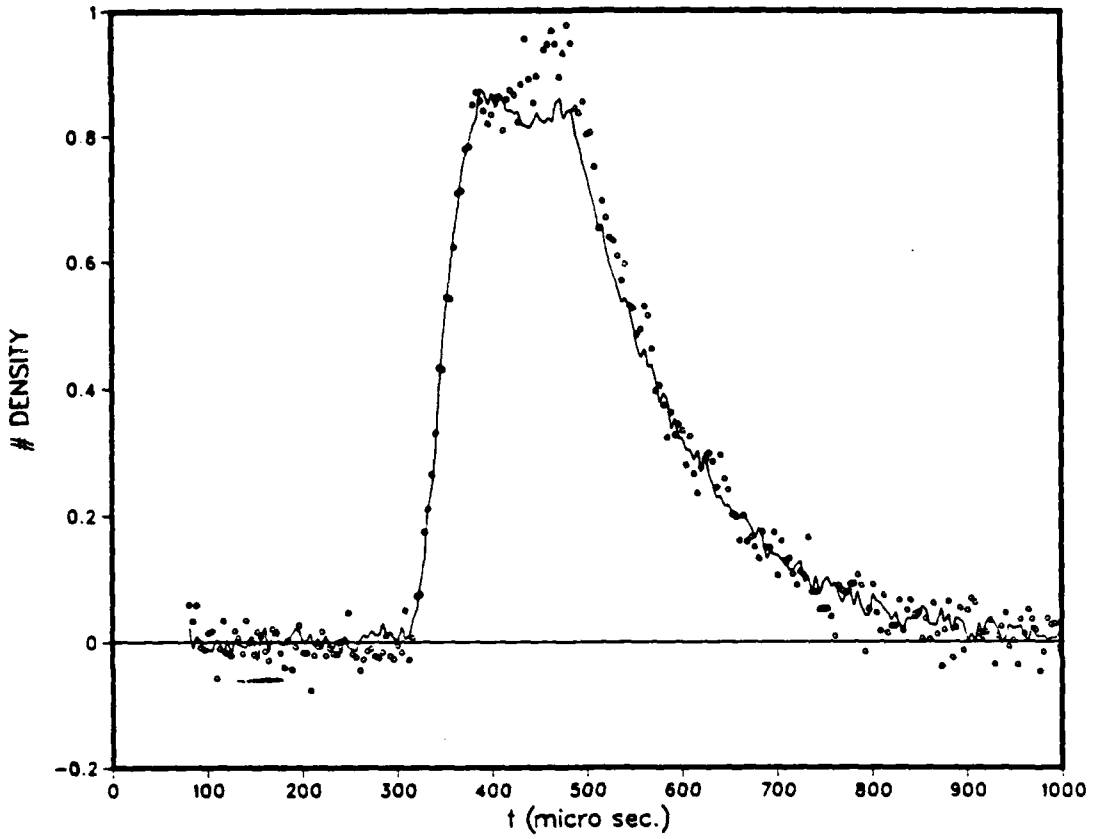

XBL 852-1157

Fig. 7.

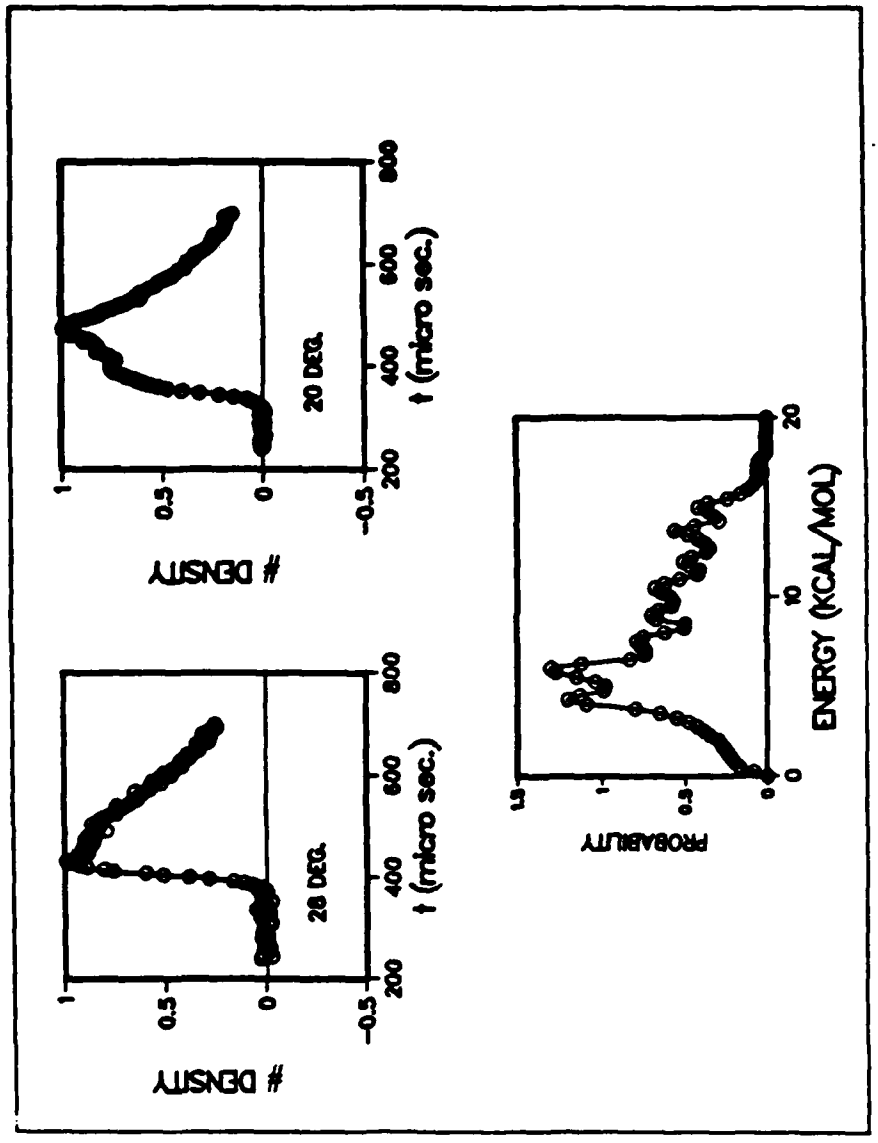
20 DEG.
28 DEG.
DENSITY
t (micro sec.)
PROBABILITY
ENERGY (KCAL/MOL)

Fig. 8.

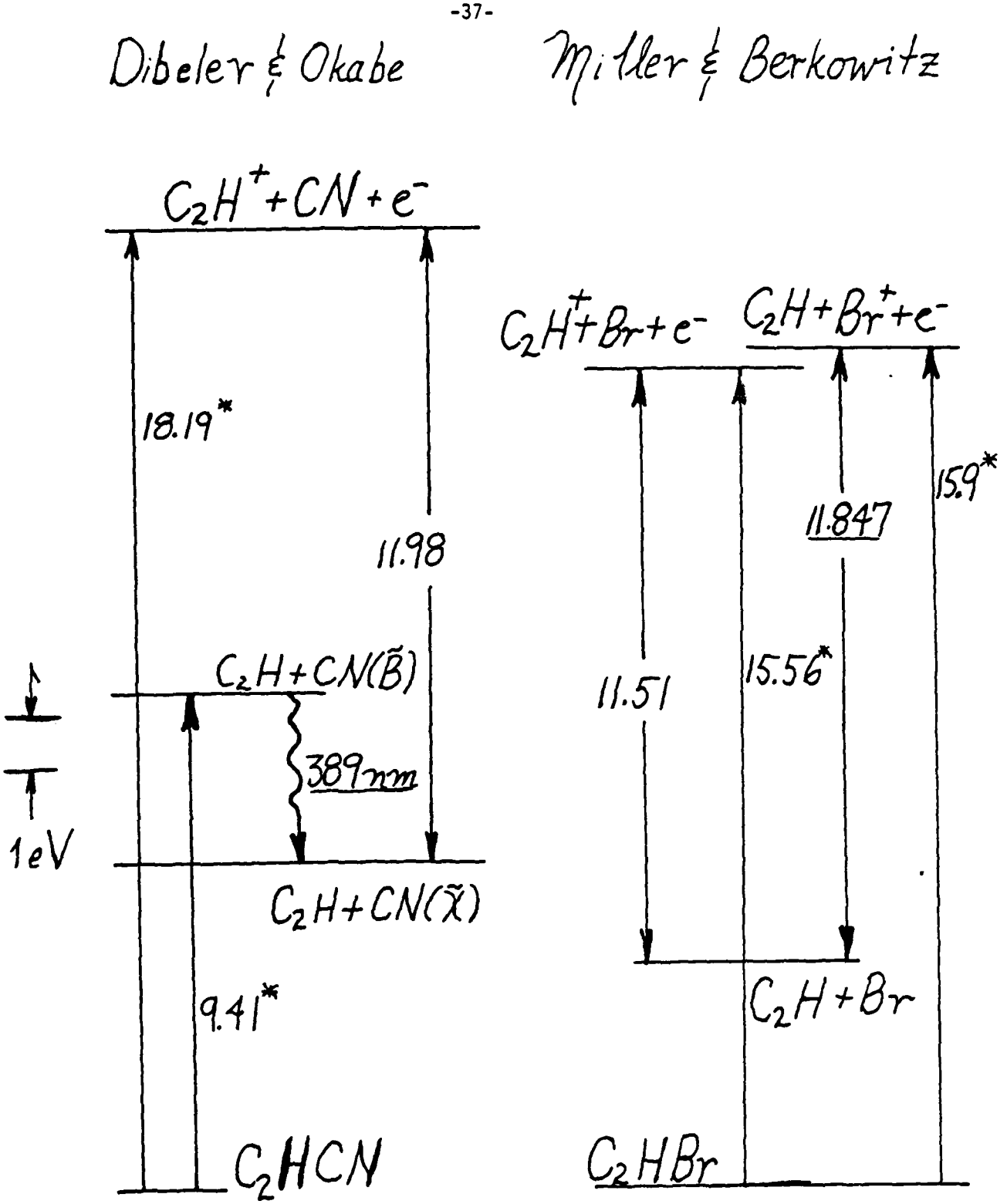
Dibeler & Okabe
Miller & Berkowitz
$C_2H^+ + CN + e^-$
18.19*
11.98
$C_2H + CN(\tilde{B})$
389nm
1eV
$C_2H + CN(\tilde{X})$
9.41*
C_2HCN
$C_2H^+ + Br + e^-$
$C_2H + Br^+ + e^-$
11.847
15.9*
11.51
15.56*
$C_2H + Br$
C_2HBr

Fig. 9.

II. THE PHOTODISSOCIATION OF CH_2BrI AT 248 AND 193 NM

The photodissociation of CH_2BrI was undertaken to continue our investigation of how the electronic nature of a particular state excited in a molecule influences the product channels by which the molecule dissociates. Although there are numerous dissociation channels for CH_2BrI which are energetically allowed at both excitation wavelengths of 193 and 248 nm, see Fig. 1,[1] our results to follow show that excitation at each wavelength produces very different branching ratios between the possible dissociation channels. Much of the data taken on this system is still under analysis, but preliminary results are presented here.

The broad ultraviolet spectrum of CH_2IBr has been recorded by S.J. Lee and R. Bersohn[2] from 200 nm to 350 nm. It consists of a broad band peaking near 270 nm which is assigned to the promotion of a nonbonding electron on the iodine to an antibonding orbital on the C-I bond, and a broad band peaking near 215 nm assigned to promotion of a nonbonding electron on the Br atom to an antibonding orbital in the C-Br bond. The bands are similar in shape to those observed in CH_3I and CH_3Br respectively, but they are considerably more intense and shifted to the red. Lee and Bersohn[2] attributed the differences to the fact that the central carbon atom has more positive charge in this dihalomethane than it does in a monohalo methane, thus stabilizing the antibonding orbitals. No spectra have been recorded near 193 nm, but it is likely that there are sharp features in this region due to Rydberg transitions on the iodine atom, as has been observed for CH_3I.[3]

Two studies of bromo-iodo alkanes are particularly relevant to this study. Lee and Bersohn investigated the photodissociation of CH_2BrI with a broad band light source extending from 240 to 340 nm with a FWHM of approximately 40 nm. They measured the mass spectrum of dissociation fragments and reported signal at I^+, Br^+, CH_2Br^+, and CH_2I^+, but not at IBr^+. There was no reported attempt to resolve HI^+ or $H^{81}Br^+$ from I^+ or Br^+. From their integrated signal at I^+ and Br^+, they derived a branching ratio between C-I and C-Br bond fission to be 5:1; the calculation involved the estimated factor that only 7 percent of the CH_2Br product formed gives signal at Br^+ and 20 percent of the CH_2I product formed gives signal at I^+. It was concluded that excitation in the n(I) → σ*(C-I) promotes only C-I Bond fission; the C-Br fission was attributed to the bandwidth of the light overlapping the n(Br) → σ*(C-Br) transition somewhat.

A recent study of the photodissociation of C_2F_5Br, C_2F_5I, and 1,2-C_2F_4BrI by Krajnovich et al.[4] investigated product channels resulting from excitation in the n(I) → σ*(C-I) and in the n(Br) → σ*(C-Br) absorption bands. The absorption spectra of Leone and coworkers from 190-400 nm show that the two broad band components of the spectrum of 1,2-C_2F_4BrI are similar in shape and position to the n(I) → σ*(C-I) absorption in C_2F_5I (peaking near 270 nm) and the n(Br) → σ*(C-Br) absorption in C_2F_5Br (still rising at 193 nm) but are considerably more intense (particularly the n(Br) → σ*(C-Br) transition). Krajnovich et al. measured the TOF and product angular distributions for excitation of the species at selected UV laser wavelengths. When 1,2-C_2F_4BrI was excited

at 248 nm and 266 nm, only C-I bond fission was observed and most or all of the iodine product was spin orbit excited $I(^2P_{1/2})$. When the molecule was dissociated at 193 nm, some of the molecules underwent primary C-I bond fission and some underwent primary C-Br bond fission in a ratio of approximately 1.7:1. The results were interpreted in terms of a fast electronic energy transfer between the C-Br and C-I bonds after a local excitation of the C-Br bond at 193 nm.

We thus endeavored to study the photodissociation of CH_2BrI at 193 nm and 248 nm to learn more about the correlation between the initial electronic state excited in bromo-iodo-alkanes and the final dissociation channels observed.

EXPERIMENTAL

The molecular beam photofragmentation apparatus has been described in detail in a previous report.[6] CH_2BrI was obtained from Fairfield Chemical Company. The molecular beam was formed by bubbling argon through a reservoir of CH_2BrI maintained at 18°C. A total stagnation pressure of 300 torr was used (5 torr CH_2BrI, 295 Ar) behind a 0.125 mm diameter nozzle. The nozzle was heated to 135°C to reduce contamination of the molecular beam by clusters. The data was checked for contributions from dissociation of clusters by repeating several measurements under the same molecular beam conditions except the reservoir of CH_2BrI was lowered to 5°C to substantially reduce the partial pressure of CH_2BrI in the beam and thus reduce cluster formation. The peak velocity of the molecular beam was 6.2×10^4 cm/sec with a FWHM of about 12 percent. The beam passed through

two skimmers and two differential pumping regions, the second skimmer defining the beam to an angular divergence of 1.5° before the molecular beam crossed the laser about 73.7 mm from the nozzle. At the crossing point the beam diameter has reached 3 mm. The beam source is rotated in a plane perpendicular to the laser beam.

The light from a pulsed Lambda Physik model EMG 103MSC excimer laser operated at 100–150 Hz was focused onto the interaction region of the molecular beam to an oblong 3 mm by 1 mm spot with a 240 mm f.l. magnesium fluoride lens. For all the data presented here the laser was unpolarized, although the polarization dependence of some of the data was measured and is being analyzed. Laser pulse energies at 193 nm, ArF gas mixture, were typically 100–150 mJ/pulse and at 248 nm, KrF gas mixture, were ~200 mJ/pulse, with pulse widths of 17 and 25 nsec respectively (quoted from Lambda Physik).

Dissociation products formed at the crossing point of the laser and molecular beam travel 36.6 cm to an electron bombardment ionizer. The ion fragments are mass selected with a quadrupole mass spectrometer and counted with a Daly detector and a multichannel scaler with respect to their flight time from the interaction region. All time-of-flight (TOF) data presented was (signal) averaged over at least 200,000 laser shots each.

RESULTS AND ANALYIS

I. Photodissociation of CH_2BrI at 248 nm

A. $CH_2BrI \xrightarrow{248\ nm} CH_2Br + I(^2P_{3/2})$ (1a)

$CH_2BrI \xrightarrow{248\ nm} CH_2Br + I(^2P_{1/2})$ (1b)

The time-of-flight (TOF) spectra of m/e=95, $CH_2\ ^{81}Br^+$, and m/e=127, I^+, are shown in Figs. 2 and 3 respectively. Both sets of TOF spectra show two narrow and fast overlapping product distributions, as well as a slow hump with a peak flight time of ~650 μsec at small laboratory angle. The I^+ TOF spectra also show a broad underlying signal. The slow hump at 650 μsec was determined to be contribution from dimer contamination in the molecular beam (see Section I.E) and the broad underlying signal in the I^+ TOF's is due to secondary photon dissociation of CH_2I product (see Section I.G) leaving the two fast and narrow peaks. The two sharp peaks in the I^+ and CH_2Br^+ TOF spectra are easily assigned to the momentum matched I and CH_2Br products from C-I bond fission, the faster one of the pair being products from bond fission producing $I(^2P_{3/2})$ and the slower one of the pair being products from bond fission producing $I(^2P_{1/2})$. The products from the bond fission giving spin orbit excited iodine atom product must channel 21.7 kcal/mole (the spin orbit splitting of iodine) of the total available energy into electronic energy. Hence, less energy is available for translation and internal vibration and rotation, and these products have smaller center-of-mass recoil velocities and hence longer arrival time in the TOF spectra.[7]

The center-of-mass recoil product translational energy distribution, $P(E_T)$, for C-I bond fission in CH_2BrI excited at 248 nm can be derived from forward convolution fitting of either the CH_2Br^+ TOF or the sharp peaks in the I^+ TOF, as the CH_2Br and I center-of-mass (c.m.) product velocities are related simply by momentum conservation. The CH_2Br^+ TOF was used initially as it is not complicated by the underlying signal from secondary dissociation. The $P(E_T)$ shown in Fig. 4 gives the fit shown in solid line in Fig. 2. This total $P(E_T)$ must be divided into two component translational energy distributions, one for production of each spin orbit state of I atom product, in order to determine a product channel branching ratio. This was done approximately by constraining the shape of each $P(E_T)$ to be similar. Although there is clearly uncertainty in the shape of the $P(E_T)$'s in the overlapping region, there is less uncertainty in the total area under each component $P(E_T)$, which determines the product channel branching ratio. Production of ground state iodine is clearly the favored channel. The $P(E_T)$'s and their fits shown in Figs. 2 and 3 give the relative probability of producing spin orbit excited I atom product in the primary bond fission to forming ground state I atom product to be 0.75:1.[11]

There are several potential pitfalls in determining product channel branching ratios from the relative area of $P(E_T)$'s that fit measured TOF spectra of products, all of which are shown to be avoided in this work. Certainly the molecular beam velocity, flight path, and ion flight time must be carefully determined so the well known transformations from $P(E_T)$ to product laboratory TOF can be carried out. More importantly, if one is determining the product channel branching ratio from the TOF spectra of a

product like CH_2Br, which has the potential of absorbing another photon and dissociating itself, one must be certain that one is not preferentially losing the CH_2Br produced in one channel over the other (this is possible because the internal state distribution of the CH_2Br product from each channel is different). Also it is possible that the more internally hot CH_2Br from dissociations producing ground state I atoms may be less likely to give parent CH_2Br^+ when ionized. All these potential problems may be eliminated by using the $P(E_T)$'s derived from the CH_2Br^+ TOF to fit the momentum matched I^+ TOF features, as was done in Fig. 3. The only remaining uncertainty is whether the probability of I $^2P_{1/2}$ being ionized per unit time in the ionizer is the same as that of I $^2P_{3/2}$. This was explicitly checked with our ionizer conditions by photodissociating CF_3I at 248 nm and checking that the same weighting of the two dissociation channels (~7 percent I $^2P_{3/2}$ is formed) fit both the CF_3^+ and the I^+ TOF spectra. Similar insensitivity of the ionization efficiency to the spin orbit excitation of I has been noted by Gorry and coworkers[8c] for their ionizer conditions. Thus our product channel branching ratio of 0.75:1 for I $^2P_{1/2}$:I $^2P_{3/2}$ only contains the relatively small uncertainty of assigning overlapping portions of each component in the TOF spectra to one or the other channel. The branching ratio does assume each channel has the same anisotropy.[11]

B. $CH_2BrI \xrightarrow{248\ nm} CH_2I + Br\ (^2P_{3/2}, {}^2P_{1/2})$ (2)

The TOF spectra of m/e=141, CH_2I^+ and m/e=81, $^{81}Br^+$, are shown in Figs. 5 and 6 respectively. The spin orbit splitting of Br atoms is

10.54 kcal/mole compared to 21.7 kcal/mole for I atoms, so one would not expect to resolve the two component dissociation channels (as was achieved for C-I fission above) given the width of the product translational energy distribution. The total $P(E_T)$ for C-Br bond fission to CH_2I + Br was derived via fitting of the CH_2I^+ TOF spectrum and is shown in Fig. 7. The corresponding fit obtained to the CH_2I product TOF is shown in solid line in Fig. 5. There is clearly a little uncertainty in the low energy side of the P(E) due to contamination of the CH_2I^+ TOF by signal from dimers (see section I.E) This $P(E_T)$ was then used to predict where signal from the momentum matched Br product would appear in the Br^+ TOF. The predicted Br^+ distribution shown in solid line in Fig. 6 matches the shape and position of the spike in the Br^+ signal. We attribute the broad underlying signal in these TOF's to secondary dissociation of some of the CH_2Br product from C-I bond fission (see Section I.F). It should be noted that some of the faster signal in the peak of the Br^+ TOF spectra could be due to CH_2Br product giving Br^+ in the ionizer, but the fraction of this contribution must be small or the shape of the fits would not match the shape of the observed peaks.

The relative intensities of the Br atom signal from C-Br bond fission and the I atom signal from C-I bond fission suggest that C-Br bond fission is a minor channel. This will be quantified after more extensive data analysis.

C. Elimination of the Possibility of Occurence of $CH_2BrI \xrightarrow{248\ nm}$ CHI + HBr (3) and $CH_2\ BrI \xrightarrow{248\ nm} CHBr + HI$ (4)

Two independent techniques were used to check for the possibility of concerted dissociation channels forming HI or HBr. First one looks for signal at HI^+ and at $H^{81}Br^+$. If any is observed one must compare it to the shape of the signal at I^+ (or Br^+ respectively) to be certain it is not m/e=127 (or 81) leaking through when the quadrupole is set to pass m/e=128 (or 82).[12] This technique assumes that if any HI or HBr is formed, they will give some parent ion in the ionizer. Second one looks for differences in the spectra of CH_2I^+ and CHI^+ and of $CH_2\ ^{81}Br^+$ and $CH\ ^{81}Br^+$ as the partner fragment of HI, CHBr, would contribute to the $CH\ ^{81}Br^+$ but not to the $CH_2\ ^{81}Br^+$ TOF (and likewise for HBr, CH_2I, and CHI). The TOF spectra taken at m/e=128, HI^+, and m/e=82, $H\ ^{81}Br^+$, are shown in Fig. 8. The TOF spectra of m/e=140, CHI^+, and 94, $CHBr^+$, are shown in Fig. 9. The very small signal at HBr^+ around 300 μsec measured at 20° could easily be due to leaking of the Br^+ through the quadrupole and the similarity of the CHI^+ and CH_2I^+ (Figs. 9 and 5) affirm that no HBr production is evident. Similarly there is no evidence for HI production, as there is no signal at HI^+ (Fig. 8) and the TOF spectra of $CH\ ^{81}Br^+$ and $CH_2\ ^{81}Br^+$ (Figs. 9 and 2) are indistinguishable.

D. *Possibility of a Tiny Fraction of* $CH_2BrI \xrightarrow{248\ nm} CH_2 + IBr$ (5)

The TOF spectrum of m/e=206, 208, IBr^+, is shown in Fig. 10. The signal is so low even at such small center-of-mass velocities when the

molecular beam TOF technique is particularly sensitive that one cannot discount the possibility this signal is due to dimers. We searched for evidence of the monomer concerted reaction two other ways. Because the momentum matched CH_2 is so much lighter than IBr, its recoil velocity would be quite fast and might be observable. Fast signal was observed in the CH^+ TOF, Fig. 11, but it was not correctly related to the IBr^+ signal by momentum conservation (this signal is assigned to CH_2 from the secondary dissociation of CH_2Br and CH_2I in Section's I.F and I.G). One can predict where the CH_2 should appear in the CH^+ TOF via conservation of momentum with the observed IBr^+ signal, this is shown by the fastest broad hump in the CH^+ spectrum. There is no signficant signal there. In addition, there is no evidence for IBr in the fragment ion mass I^+ TOF spectra; at 10° (Fig. 3) the peak would arrive at ~500 μsec, between the I product signal from C-I bond fission and the hump from dimer contamination.

It should be stated that if any IBr were formed with a total translational energy release of less than ~4.4 kcal/mole it would not recoil away from the molecular beam with a large enough velocity to be detected. The CH_2 product from $CH_2BrI \rightarrow CH_2 + IBr$ could however be detected at 20° with as little as 0.04 kcal/mole release to translation, but might be difficult to pick out in the congested CH^+ spectrum.

E. Identification of Signal from Dissociation of Dimer Contamination in the Molecular Beam.

Although the fraction of CH_2BrI associated as dimers in the molecular beam is probably very small (the reservoir of CH_2BrI was held at 18°C and the nozzle was heated to 135°C), some contamination of the TOF spectra from dissociation of clusters can be observed at small angles. Cluster fragments that recoil with small c.m. velocities are constrained to be concentrated in a small laboratory angular range about the molecular beam, so although their signal is not observed at large angles we are particularly sensitive to their signal at 10°. Signal at low recoil velocities with respect to the molecular beam (assuming primary fragments) made significant contribution to three TOF spectra. These spectra were explicitly checked for contamination from dissociation products of clusters by repeating the TOF spectra with a substantial decrease in the partial pressure of CH_2BrI in the molecular beam as described in the experimental section. The increase in the beam velocity was very small, as the seeding ratio for the regular data was already small, so the TOF's can be directly compared.

The TOF spectra of m/e=81,94 and 127 at 10° obtained with reduced polymer contribution to the molecular beam are shown in Fig. 12. Under the new beam conditions all the signal is substantially reduced, but the ratio of monomer molecules to clusters in the moleclar beam is significantly increased. Thus any signal from cluster parent molecules will be reduced in intensity with respect to signal from dissociation of monomers. Comparing the m/e=127 TOF at 10° here in Fig. 12 with that in Fig. 3, one sees that the feature near 650 μsec flight time is clearly due to dissociation of

clusters. Likewise the 20° spectrum of m/e=94 shows signal from dimers around 650 μsec. The m/e=81 spectra shows no change, however. The slow signal on this spectra is assigned to the Br from secondary dissociation of CH_2Br product below.

F. Secondary Dissociation of CH_2Br Product, $CH_2Br \xrightarrow{248\ nm} CH_2 + Br$ (5)

The TOF at m/e=81, $^{81}Br^+$ (Fig. 6), shows broad signal at faster and at slower times than the CH_2Br product arrival time (which is toward the fast side of the Br signal from C-Br bond fission indicated in solid line). Such a broad underlying signal is characteristic of secondary dissociation of a product. After primary C-I bond fission which requires 55 kcal/mole, the CH_2Br product formed cannot be left with enough internal energy to undergo unimolecular dissociation to CH_2 + Br. Its secondary dissociation must occur via absorption of another photon. In a previous experiment in this laboratory on the photodissociation of CF_2Br_2 at 248 nm,[13] the CF_2Br product from C-Br fission absorbed another photon and dissociated to CF_2 + Br, thus it is not surprising that highly internally excited CH_2Br radicals also absorb at 248 nm and dissociate.

Modeling a secondary dissociation such as this involves calculating the laboratory velocity flux distribution of the CH_2Br parent product molecules from primary C-I fission, then inputting a guessed $P(E_T)$ for dissociation to CH_2 + Br to account for the recoil of CH_2 and Br from each other. The final Br laboratory velocity is the vector sum of the molecular beam velocity, c.m. recoil velocity of CH_2Br from I and the c.m.

recoil velocity of Br from CH_2. This calculation is performed for the secondary dissociation of CH_2I below, but was not attempted for CH_2Br because of the large range of laboratory velocities of the CH_2Br product. However, the similarity between the secondary dissociation signal of Br from CH_2Br, which peaks at faster and slower arrival times than the CH_2Br parent, and the secondary dissociation signal observed by Krajnovich, et al.[13] in the CF_2Br_2 TOF data is marked and expected.

A simple calculation was made to assure that the assignment of the underlying signal in the Br^+ TOF spectrum to reaction (5) is consistent with conservation of energy and momentum. If one asks how much energy would have to go into translation in the dissociaton of $CH_2Br \rightarrow CH_2 + Br$ for the Br to reach the shortest observed arrival time at 10° of 180 μsec, one calculates 52 kcal/mole for the Br originating from CH_2Br in the peak of the $CH_2Br + I$ translational energy distribution.[14] Whether the primary and secondary photons absorbed can provide all the necessary energy is easily calculated:

$$\text{Required energy} = E_{T_{I+CH_2Br}} + D_{o_{I-CH_2Br}} + E_{T_{CH_2+Br}} + D_{o_{Br-CH_2}}$$

$$= 19 + 55 + 52 + (67) \simeq 193 \text{ kcal/mole}$$

$$2E_{h\nu} = 230 \text{ kcal/mole} > 193 \text{ kcal/mole.}$$

One also calculates that the CH_2 product from the secondary dissociation of CH_2Br which releases 52 kcal/mole to translation would have a total flight time (flight time to ionizer + ion flight time) of 67 μsec. This corresponds to within a few μsec to the fast side of the previously unassigned sharp spike in the CH + TOF of Fig. 11. Thus CH^+

signal is observed which is momentum matched with the fastest Br^+ signal observed, as required for reaction 5, and the observed product velocities are accessible with the available energy.

G. Secondary Dissociation of CH_2I Product, $CH_2I \xrightarrow{248\ nm} CH_2 + I$ (6).

The TOF spectrum of m/e=127, I^+, contains a broad underlying signal which we assign to the secondary dissociation of CH_2I product from C-Br bond fission. As for CH_2Br secondary dissociation, the CH_2I product cannot have enough internal energy after the C-Br bond fission to dissociate unimolecularly. It must dissociate via absorption of another photon.

The shape of the secondary dissociation TOF signal was calculated from a possible $P(E_T)$ for rxn. 6 as follows. We assumed first that all the CH_2I product from C-Br bond fission had equal probability of absorbing another photon and dissociating to $CH_2 + I$. This assumption is unlikely to be strictly true, but unless, for instance, the CH_2I product in the fast side of the distribution has a much higher likelihood of undergoing secondary dissociation than the CH_2I in the slow side, the effect of a varying dissociation probability across the CH_2I primary product distribution would not affect the secondary TOF calculation significantly. No obvious depletion of one part of the CH_2I TOF is evident when one compares the shape of the momentum matched Br spike in the Br^+ TOF spectra (Fig. 6) with the shape predicted in solid line from the velocities of the observed CH_2I product. Second, one calculates the laboratory velocity flux of the CH_2I product from which the $CH_2 + I$ fragments will originate. This is a simple extension of our usual fitting procedure with one exception. The

scattered CH_2I product is constrained by symmetry to have an isotropic c.m. angular distribution with respect to Θ, the angle in the plane perpendicular to the unpolarized laser beam. However, the c.m. angular distribution with respect to the ϕ angle cannot be derived from TOF measurements with an unpolarized laser and the geometry of the present apparatus. In the absence of measurement of this anisotropy we assumed this distribution to be isotropic. It remains to be checked how different the calculation results are if the C-Br bond fission is strongly anisotropic. Finally, the recoil of the CH_2 from I in the secondary dissociation (6) is accounted for from each CH_2I parent molecule; we also assumed this to be isotropic. A $P(E_T)$ is guessed for the dissociation and a TOF at I^+ is calculated, then the $P(E_T)$ is refined until the fit is good. The $P(E_T)$ shown in Fig. 13 for rxn. 6 gave the acceptable fit to the underlying signal shown in Fig. 3. Because there are other contributions to these spectra, uncertainty in what signal should be fit is evident. It is, however, certain that the secondary dissociation signal should extend underneath the primary I signal or the relative heights of the two components would not be well fit by the $P(E_T)$ derived for rxns. 1a and 1b from the CH_2Br^+ spectra.

II. Photodissociation of CH_2BrI at 193 nm

The TOF and angular distribution data taken at an excitation wavelength of 193 nm are still being analyzed, but several prelimary results are suggested.

A. C-Br bond fission, $CH_2IBr \xrightarrow{193\ nm} CH_2I + Br$, is a major dissociation channel, as evidenced by the m/e=141, CH_2I^+, TOF shown in Fig. 14. The P(E) that fit this "remaining"[15] CH_2I product signal is shown in Fig. 15.

B. C-I bond fission, $CH_2IBr \xrightarrow{193\ nm} CH_2Br + I$, is also a dissociation channel. A sharp spike is seen in the weak m/e=91-95, CH_nBr(n=0,1,2) TOF spectrum shown in Fig. 16. The P(E) that fit this "remaining"[15] CH_nBr sharp spike is shown in Fig. 17.

C. *Concerted elimination* of IBr, $CH_2IBr \xrightarrow{193\ nm} CH_2 + IBr$ is a significant dissociation channel. The IBr product is detected at m/e=206, 208, IBr^+, in Fig. 18. The thermodynamics indicate that the observed IBr is very likely to be electronically excited. The P(E) for IBr elimination is shown in Fig. 19.

D. Concerted elimination of HI, $CH_2IBr \rightarrow HI + CHBr$, may be occurring. It is impossible to fit all the signal in the I^+ and Br^+ TOF data (shown in a previous report, ref. 6) with solely contributions from products of the three processes above. The remaining signal can be approximately fit with only one additional channel if H_nI, n=0,1, recoils from CH_nBr(n=2,1). Since a C-I bond fission channel that releases so little energy to translation is unlikely, HI elimination may be the explanation for the unassigned signal in the I^+ and Br^+ TOF spectra.

E. Some or all of the I and Br atoms formed from C–halogen bond fission at 193 nm are spin orbit excited.

F. The $CH_2IBr \rightarrow CH_2 + I + Br$ endoergicity estimate of 123 kcal/mole is an underestimate by at least 10 kcal/mole. We observe CH_2I product at $E_T < 5$ kcal/mole. Assuming the C–Br bond strength in CH_2BrI is the same as that in CH_3Br, 67.7 kcal/mole, that leaves $148(E_{h\nu}) - 67.7 - 5 = 75.3$ kcal/mole for the electronic excitation of Br and internal excitation of CH_2I. Even if the Br from this dissociation of $E_T = 5$ kcal/mole is in the $^2P_{1/2}$ state, the CH_2I still has about 65 kcal/mole of internal energy. The 123 kcal/mole endoergicity assumes that the $I-CH_2$ bond strength is 55 kcal/mole, as it is in CH_3I, but this must be underestimated by at least ~10 kcal/mole since we observe CH_2I product with 65 kcal/mole of internal energy. Thus the C–I bond in CH_2I should be considerably stronger than in CH_3I and the endoergicity of $CH_2IBr \rightarrow CH_2 + I + Br$ is probably closer to 133 kcal/mole.

REFERENCES

1. The heats of formation of a variety of chemical species used to calculate the enthaplies shown in Fig. 1 were obtained from: Rosenstock et al., J. of Phys. and Chem. Ref. Data, 6, Suppl. 1, I-774 (1977).

2. S. J. Lee and R. Bersohn, J. Phys. Chem. 86, 728 (1982).

3. R. A. Boschi and D. R. Salahub, Mol. Phys. 24, 289 (1972).

4. D. Krajnovich, L. J. Butler, and Y. T. Lee, J. Chem. Phys. 81, 3031 (1984).

5. W. H. Pence, S. L. Baughaum, and S. R. Leone, J. Phys. Chem. 85, 3844 (1981).

6. ONR/NRL Workshop on Energetic Materials Initiation Fundamentals, 30 October-1 November 1984.

7. This is a result of both sets of products recoiling down a similar repulsive energy surface except for the difference in final product energies. The complete or partial resolution in TOF spectra of products from carbon-halogen bond fission producing two spin orbit states of halogen atom product has been previously oberved for CH_3I,[8a-e] CF_3I,[8b,9] CH_3Br,[8b] CF_3Br,[9] CD_3I,[8b] and 1,2-C_2H_4ClI.[10]

8. a) R. K. Sparks, K. Shobatake, L. R. Carlson, and Y. T. Lee, J. Chem. Phys. 75, 3838 (1981); b) G. N. A. van Veen, "Excited Species from Photofragmentation," Ph.D. Thesis (1984); c) M. D. Barry and P. A. Gorry, Mol. Phys. 52, 461 (1984); d) S. J. Riley and K. R. Wilson, Disc. Faraday Soc. 53, 132 (1972); e) M. Dzvonik, S. Yang, and R. Bersohn, J. Chem. Phys. 61, 4408 (1974).

9. L. J. Butler, A. Wodtke, E. Hintsa, and Y. T. Lee, unpublished.

10. T. K. Minton, P. Felder, R. J. Brudzynski, and Y. T. Lee, J. Chem. Phys. 81, 1759 (1984).

11. This product channel branching ratio assumes both dissociation channels have the same anisotropy with respect to the laser electric vector. The anisotropies of the C-I bond fission channels producing $I^2P_{1/2}$ and $I^2P_{3/2}$ in CH_3I excited at 248 and 266 nm are equal. Preliminary angular distribution measurements of I from CH_2BrI at 248 nm indicate the same is true here.

12. An alternative way is to set the resolution so high that any leakage is effectively stopped, but then a lack of signal is ambiguous since the transmission of the quadrupole is reduced as the resolution is raised.

13. D. Krajnovich, Z. Zhang, L. Butler, and Y. T. Lee, J. Phys. Chem. 88, 4561 (1984).

14. It was explicitly checked with a simple classical calculation that the C-I bond fission imparted enough rotation to the CH_2Br fragment that the recoil angle of the Br would not be constrained to be at a specific angle from the recoil direction of the CH_2Br from I. The sum of the orbital angular momentum of the departing CH_2Br and I fragments will determine the spin angular momentum imparted to the CH_2Br by angular momentum conservation. Assuming the fragments leave the c.m. at an impact parameter estimated from the geometry of the molecule with velocities derived from the peak of the TOF spectra, the CH_2Br will be made to rotate with a period of 5.6×10^{-11} sec/revolution. At

our dissociating pulse energies/cm^2 the CH_2Br fragment could rotate hundreds of times before absorbing a photon (assuming a cross section of $\sim 10^{-18}$ cm^2).

15. The stipulation "remaining" is added because a 193 nm photon contains 148 kcal/mole of energy, enough to form CH_2I and CH_2Br products from some dissociations with enough internal energy to unimolecularly dissociate to CH_2 + X. In particular, the CH_2Br and CH_2I products from primary dissociations producing ground state halogen atoms should all undergo secondary dissociation and will not contribute to the CH_2X spectra.

FIGURE CAPTIONS

Fig. 1. Energetically allowed dissociation channels of CH_2BrI excited at 193 and 248 nm. a) the C-I and C-Br bond dissociation enthalpies are assumed to be the same as that in CH_3I and CH_3Br calculated from heats of formation given in ref. 1. b) The HI and HBr elimination channel endothermicities were calculated from the C-I and C-Br energies estimated above, the H, I and Br heats of formation from ref. 1 and the assumption that the enthalpy of $CH_2X \rightarrow CHX + H$ (X=I,Br) are the same as that for $CH_3 \rightarrow CH_2 + H$ calculated from ref. 1. c) The enthalpy for $CH_2BrI \rightarrow CH_2 + I + Br$ is crudely estimated assuming the C-X bond strengths (X=I,Br) in CH_2X equals the C-X bond strengths in CH_3X. The slow CH_2I product observed at 193 nm excitation indicates that this underestimates the $X-CH_2$ bond strength by ~10 kcal/mole (given that the calculation in (a) is close). The IBr elimination channel enthalpy is calculated from the above suspect value and the enthalpy of $I + Br \rightarrow IBr$ from ref. 1.

Fig. 2. CH_2BrI at 248 nm: Product TOF spectra taken at m/e=95, $CH_2\ ^{81}Br^+$, at a source to detector angle of 20°. o Experimental points, ———— best calculated fit to the data, obtained by adding the two components ——— — ——— of CH_2Br product from reactions 1a and 1b, calculated from the two component $P(E_T)$ shown in Fig. 4.

Fig. 3. CH_2BrI at 248 nm: Product TOF spectra taken at m/e=127, I^+, at three source to detector angles of 10°, 20°, and 30°. o Experimental data. ———— fit calculated as the sume of the individual contributions of I $^2P_{3/2}$ (—— — ———, shorter arrival time), I $^2P_{1/2}$ (—— – ———, longer arrival time) (rxns. 1a and 1b) and I product of CH_2I secondary dissociation (— — —). The contributions from rxns. 1a and 1b are calculated from the two component $P(E_T)$ shown in Fig. 4 which was derived from the $CH_2Br \rightarrow$ TOF spectrum (Fig. 2) The secondary dissociation contribution was calculated from the $P(E_T)$ shown in Fig. 14, see Section I.G.

Fig. 4. Center-of-mass product translational energy distribution for $CH_2BrI \xrightarrow{248\ nm} CH_2Br + I$. The two component $P(E_T)$'s shown as ———— show the assumed shape of each component channel producing I $^2P_{1/2}$ (lower translational energies) and I $^2P_{3/2}$ (higher translational energies). This $P(E_T)$ was derived from forward convolution fitting of the CH_2Br^+ TOF shown in Fig. 2 and was used to fit the I contribution from primary dissociation in the I + TOF spectra of Fig. 3. The branching ratio for formation of I $^2P_{1/2}$:I $^2P_{3/2}$ is determined under that uncertainty to be 0.75:1 from the relative areas under each $P(E_T)$ with the assumption that the anisotropy is the same for each channel. See text in Section I.A and ref. 7. Because the laser is perpendicular to the source detector

plane and unpolarized, no anisotropy parameter is needed to calculate the shape of the laboratory TOF data from the $P(E_T)$, only the relative scaling of two $P(E_T)$'s is affected.

Fig. 5. CH_2BrI at 248 nm: Product TOF spectra taken at m/e=141, CH_2I^+, at a source to detector angle of 20°. o Experimental points. ———— fit to the data calculated for CH_2I product from rxn. 2 from the $P(E_T)$ shown in Fig. 7.

Fig. 6. CH_2BrI at 248 nm: Product TOF spectra taken at m/e=81, $^{81}Br^+$, at three source to detector angles of 10°, 20°, and 30°. o Experimental points. ———— shape of Br product contribution from C-Br primary bond fission (rxn. 2) calculated from the $P(E_T)$ shown in Fig. 7 derived from the CH_2I TOF of Fig. 5.

Fig. 7. Center-of-mass product translational energy distribution for $CH_2BrI \xrightarrow{248\ nm} CH_2I + Br$. Derived from forward convolution fitting of the CH_2I product TOF of Fig. 5.

Fig. 8. CH_2BrI at 248 nm: Product TOF spectra taken at m/e=82, $H^{81}Br^+$, top, and m/e=128, HI^+ bottom at a source to detector angle of 20°. Baseline was calculated from averaging counts in time range between 2 and 100 μsec after the dissociating laser pulse. o Experimental points.

Fig. 9. CH_2BrI at 248 nm: Product TOF spectra taken at m/e=140, CHI^+, top, and m/e=94, $CH^{81}Br^+$, bottom, at a source to detector angle of 20°. o Experimental points.

Fig. 10. CH_2BrI at 248 nm: Product TOF spectra taken at m/e=206, 208, $I^{79}Br^+$ at at source to detector angle of 10°. The assumed shape of the signal shown in solid line was used to calculate the shape of the signal that would be observed at CH^+ (see Fig. 11) if the IBr^+ signal is due to concerted elimination of IBr (rxn. 5). o Experimental points.

Fig. 11. CH_2BrI at 248 nm: Product TOF spectra taken at m/e=13, CH^+, at a source to detector angle of 20°. The $P(E_T)$'s shown in Figs. 4 and 7 which are derived from other TOF spectra were used to calculate where signal would be observed from CH_2I (_____ . _____) and CH_2Br (—— —— ——) respectively in this TOF. The hump at short arrival times shows where one would expect CH_2 from rxn. 5 if the signal observed in Fig. 10 were IBr product. The fast data shown without a fit is attributed to CH_2 from the secondary dissociation of CH_2Br and CH_2I products (see Section I.F and I.G).

Fig. 12. CH_2BrI at 248 nm: Product TOF spectra taken with special molecular beam conditions to reduce clusters in the beam. TOP, taken at m/e=127, I^+ at a source to detector angle of 10°. Middle, taken at m/e=81, $^{81}Br^+$ at a source to detector angle of 10°. Bottom, taken at m/e=94, $CH^{81}Br^+$, at a source to detector angle of 20°. o Experimental points.

Fig. 13. Center-of-mass product translational energy distribution used to fit the I signal in the I^+ TOF (Fig. 3) from the secondary dissociation of CH_2I rxn. 6. See Section I.G for discussion of assumptions in fitting the secondary dissociation signal.

Fig. 14. CH_2BrI at 193 nm: Time-of-flight data taken at m/e=141, CH_2I^+, at a source to detector angle of 20°. o Experimental points. ———— fit to the remaining[15] CH_2I signal calculated from the $P(E_T)$ shown in Fig. 15.

Fig. 15. Center-of-mass translational energy distribution for $CH_2BrI \xrightarrow{193\ nm} CH_2I + Br$, for which the CH_2I is left with little enough internal energy to be stable. The P(E) was used to fit the CH_2I signal in Fig. 14.

Fig. 16. CH_2BrI at 193 nm: Time-of-flight data taken at m/e=91-95, CH_nBr^+ (n=0,1,2). o Experimental points. ———— fit to the signal attributed to stable CH_2Br product from C-I bond fission.

Fig. 17. Center-of-mass product translational energy distribution for $CH_2BrI \xrightarrow{193\ nm} CH_2Br + I$ for which CH_2Br is left with little enough internal energy to be stable. The P(E) was used to fit the signal attributed to CH_2Br signal in Fig. 16.

Fig. 18. CH_2BrI at 193 nm: Time-of-flight data taken at m/e=206,208. o Experimental points. ———— fit calculated from the P(E) shown in Fig. 19.

Fig. 19. Center-of-mass product translational energy distribution for $CH_2BrI \xrightarrow{193\ nm} CH_2 + IBr$, for which the IBr survived secondary dissociation to I + Br. IBr may be lost via predissociation if it has >41 kcal/mole of internal energy or via absorption of a 193 nm photon.

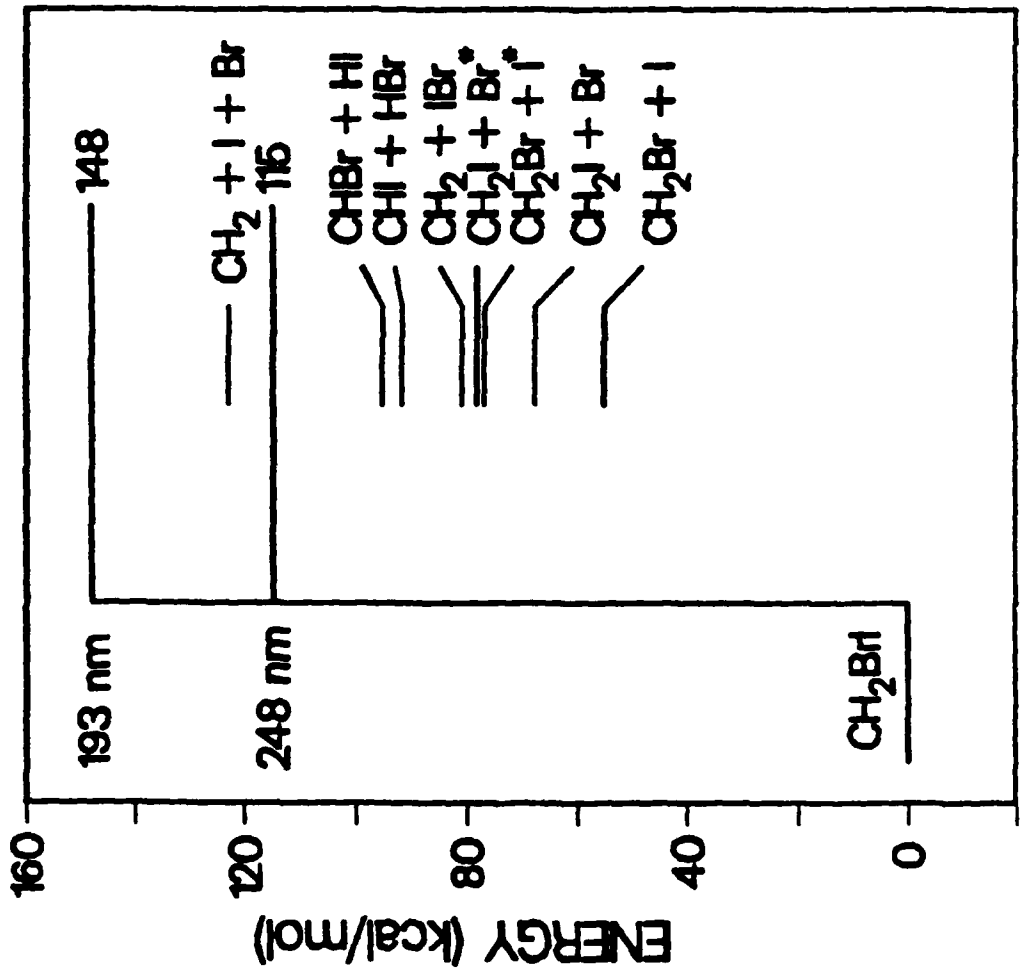
ENERGY (kcal/mol)
160
120
80
40
0
193 nm
248 nm
148
115
$CH_2 + I + Br$
CH_2BrI
CHBr + HI
CHI + HBr
$CH_2 + IBr^*$
$CH_2I + Br^*$
$CH_2Br + I^*$
$CH_2I + Br$
$CH_2Br + I$

Fig. 1

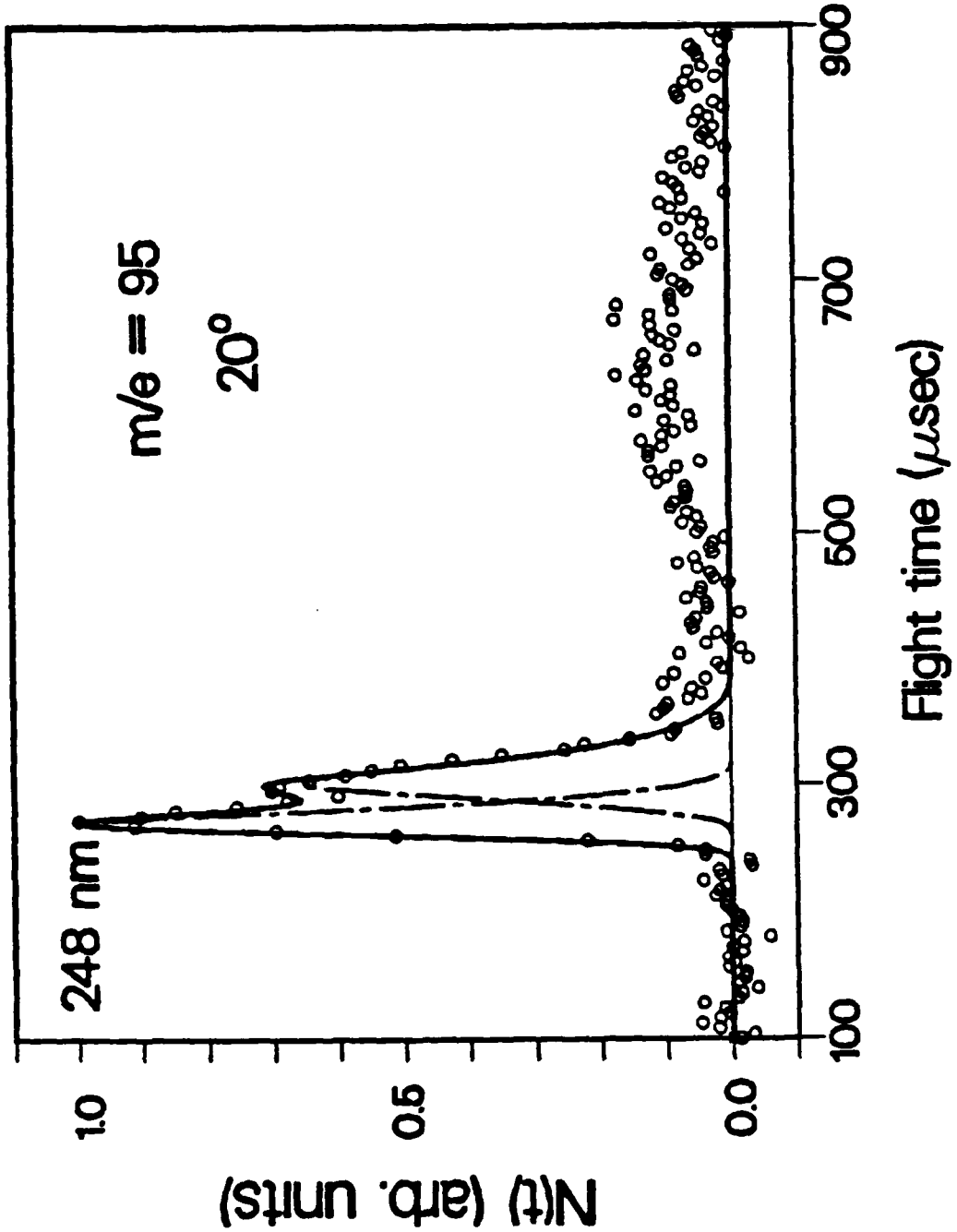
248 nm
m/e = 95
20°
N(t) (arb. units)
1.0
0.5
0.0
100
300
500
700
900
Flight time (μsec)

Fig. 2.

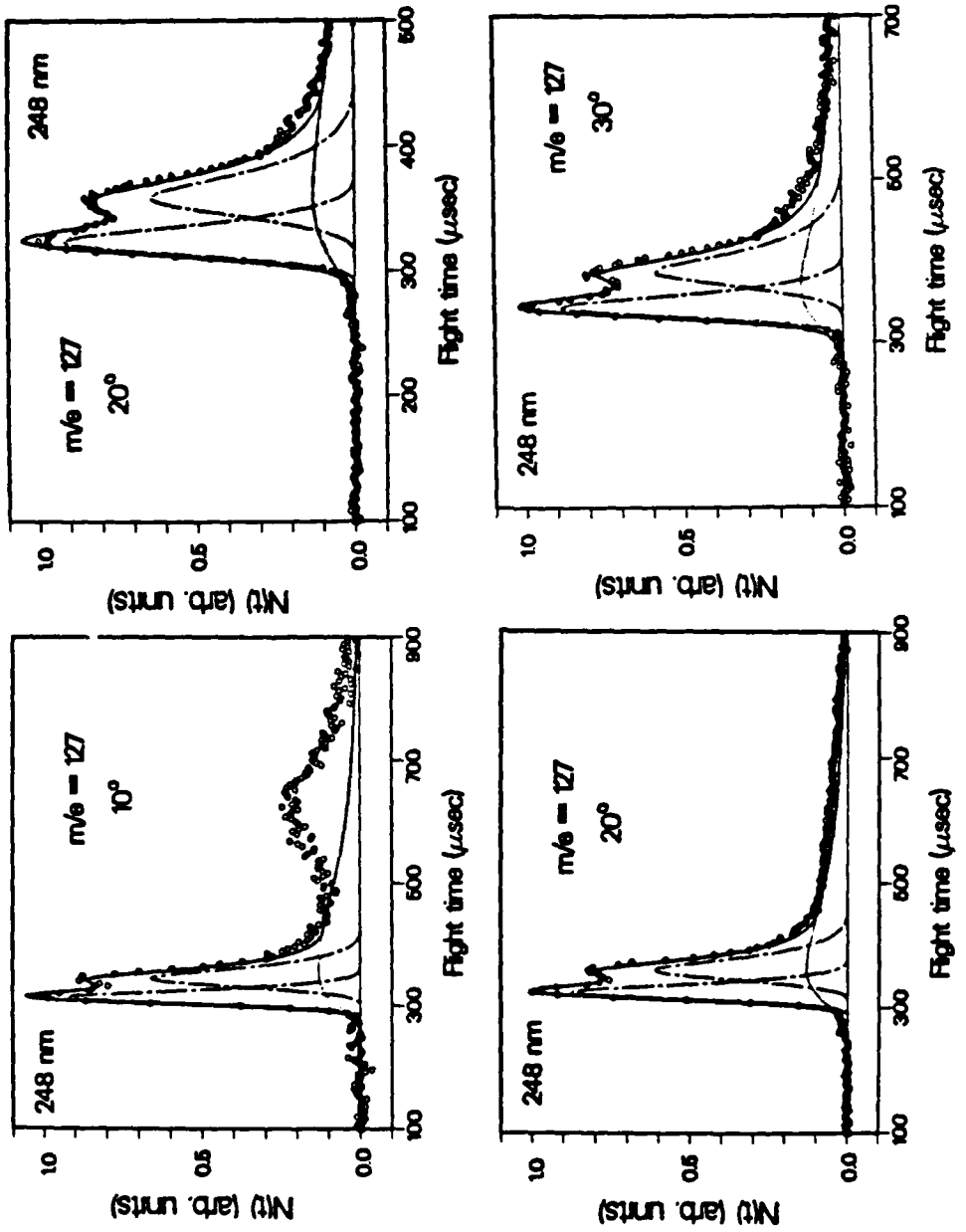
248 nm
m/e = 127
20°
N(t) (arb. units)
Flight time (μsec)
248 nm
m/e = 127
30°
N(t) (arb. units)
Flight time (μsec)
248 nm
m/e = 127
10°
N(t) (arb. units)
Flight time (μsec)
248 nm
m/e = 127
20°
N(t) (arb. units)
Flight time (μsec)

Fig. 3.

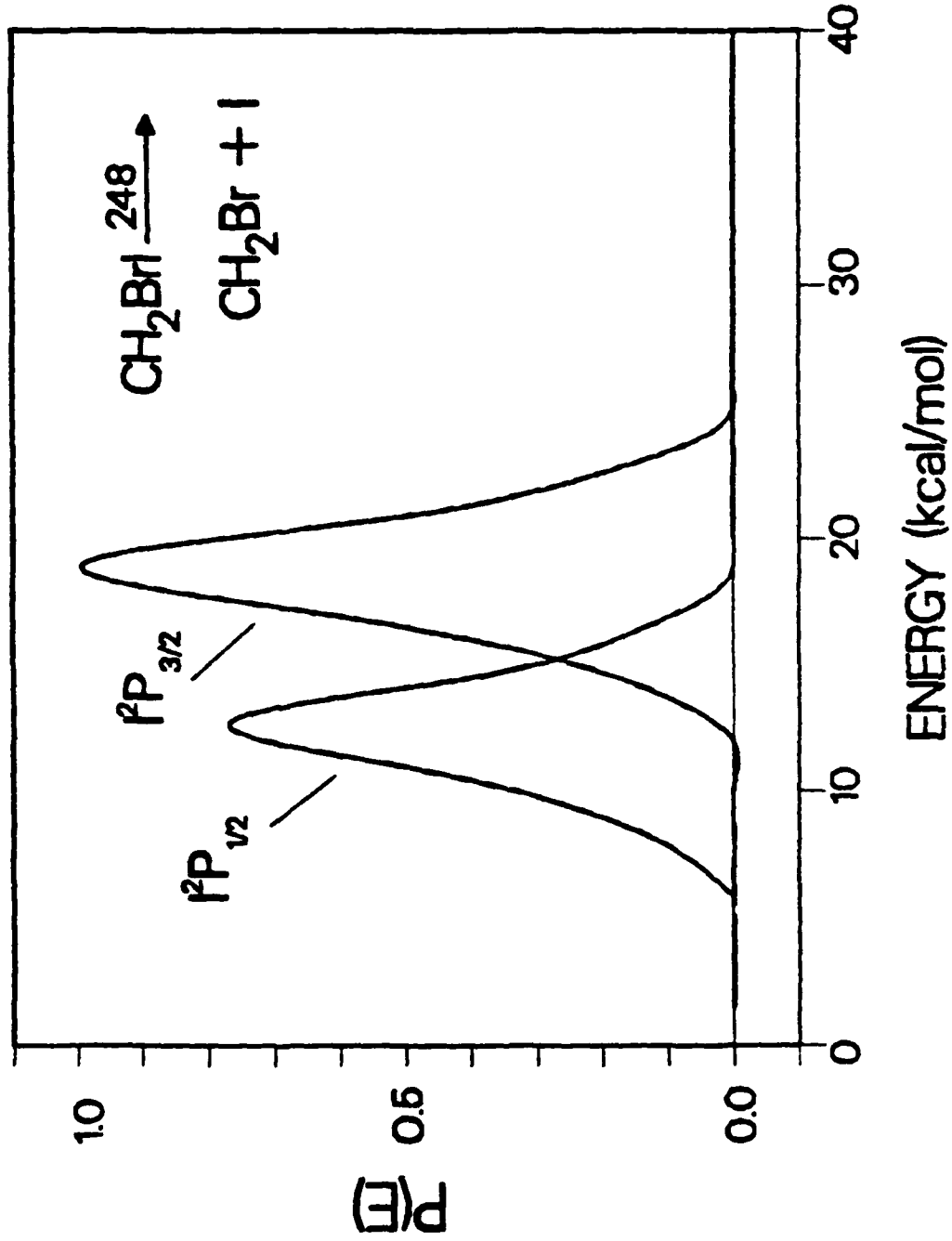
$CH_2BrI \xrightarrow{248} CH_2Br + I$
$^2P_{3/2}$
$^2P_{1/2}$
P(E)
1.0
0.5
0.0
0
10
20
30
40
ENERGY (kcal/mol)

Fig. 4

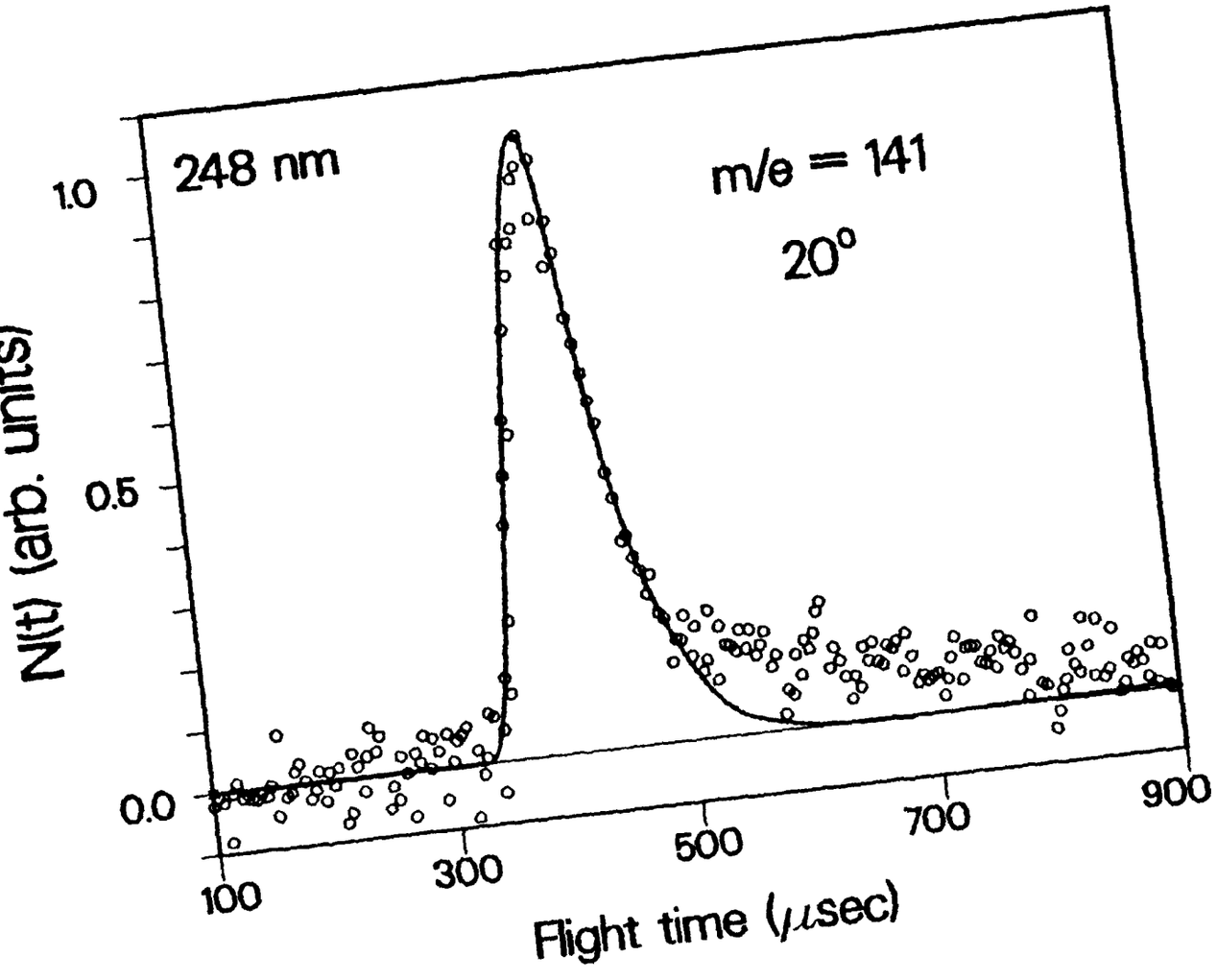
248 nm
m/e = 141
20°
1.0
0.5
0.0
N(t) (arb. units)
100
300
500
700
900
Flight time (μsec)

Fig. 5.

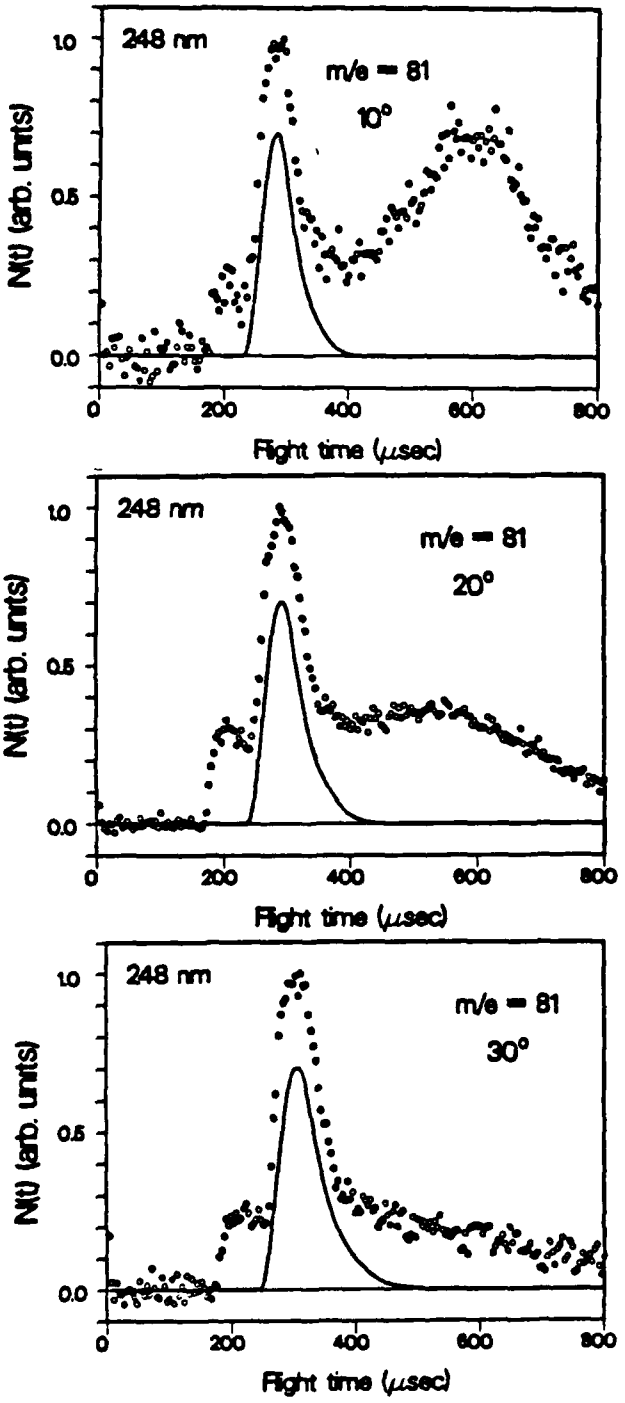
248 nm
m/e = 81
10°
N(t) (arb. units)
1.0
0.5
0.0
0
200
400
600
800
Flight time (μsec)
248 nm
m/e = 81
20°
N(t) (arb. units)
1.0
0.5
0.0
0
200
400
600
800
Flight time (μsec)
248 nm
m/e = 81
30°
N(t) (arb. units)
1.0
0.5
0.0
0
200
400
600
800
Flight time (μsec)

Fig. 6

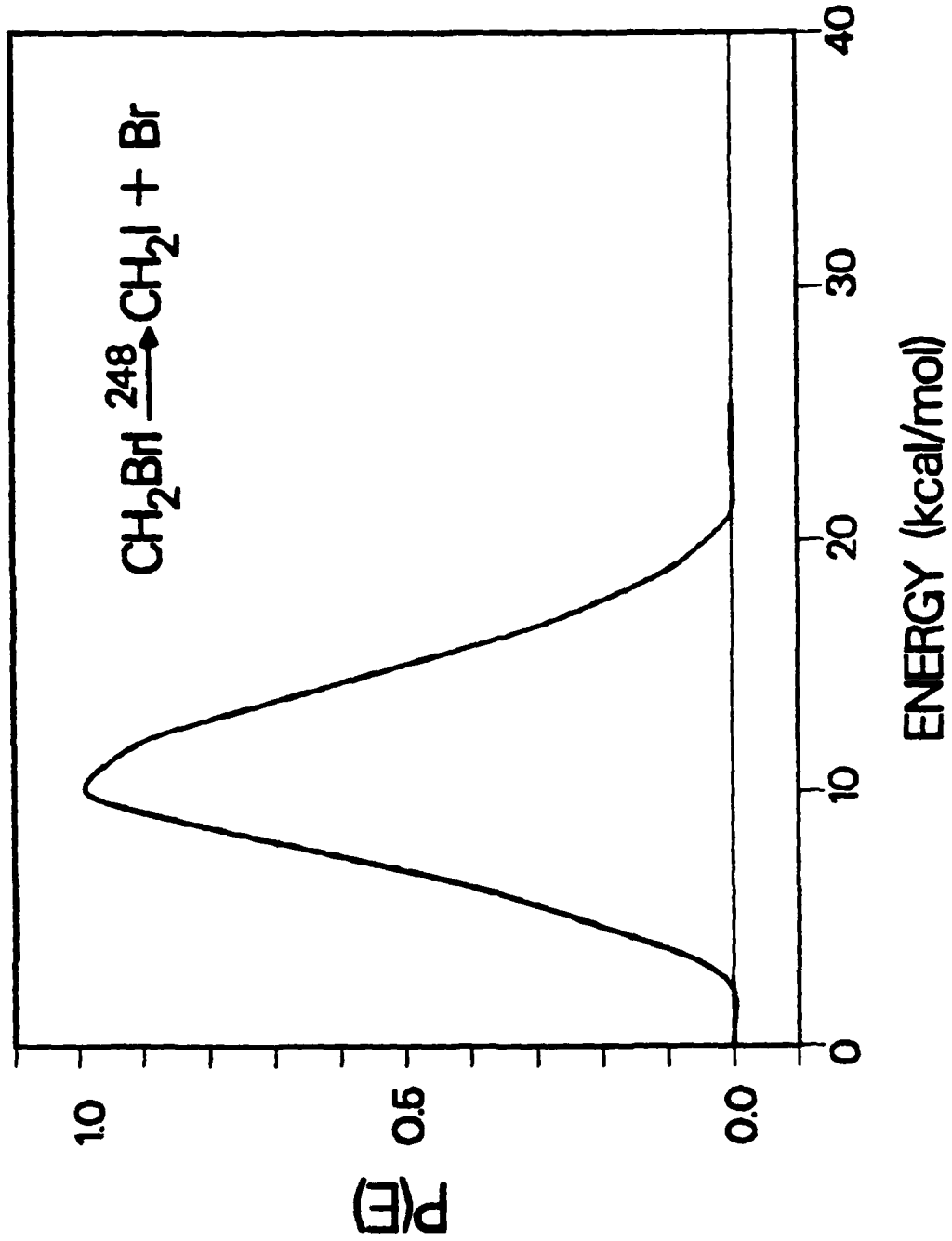
$CH_2BrI \xrightarrow{248} CH_2I + Br$
P(E)
1.0
0.5
0.0
0
10
20
30
40
ENERGY (kcal/mol)

Fig. 7

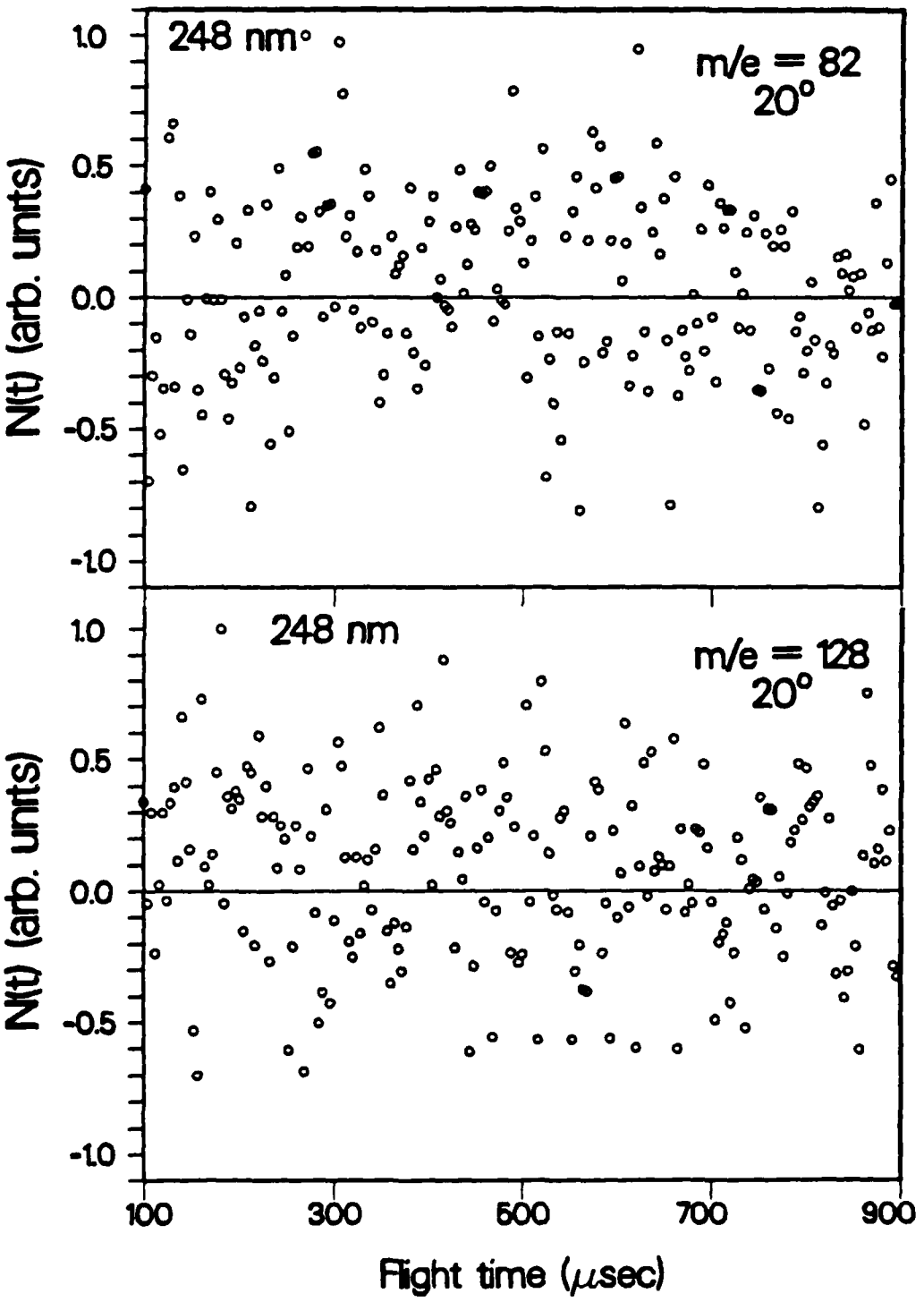
248 nm
m/e = 82
20°
248 nm
m/e = 128
20°
N(t) (arb. units)
N(t) (arb. units)
1.0
0.5
0.0
-0.5
-1.0
100
300
500
700
900
Flight time (μsec)

Fig. 8

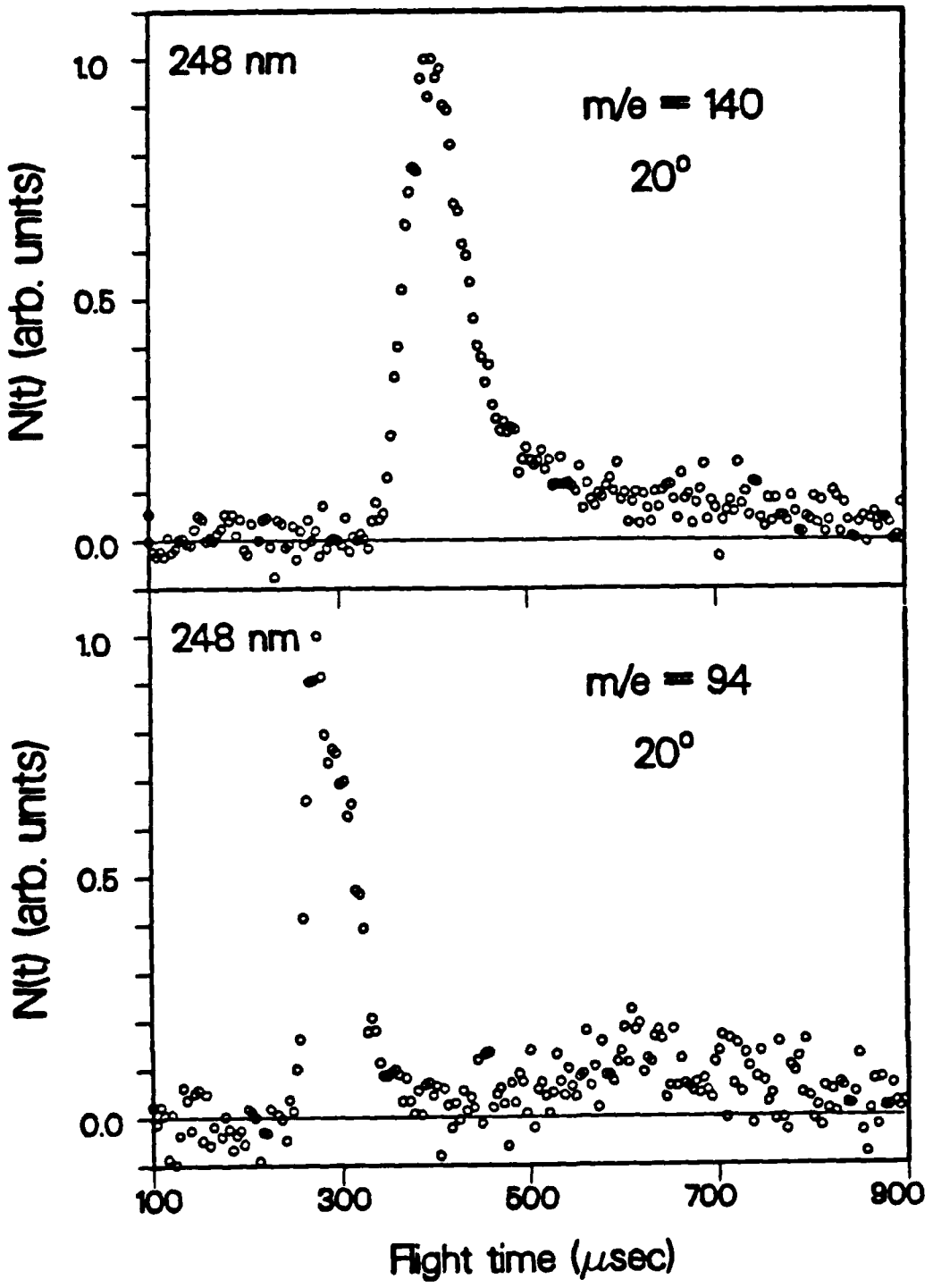
248 nm
m/e = 140
20°
1.0
0.5
0.0
N(t) (arb. units)
248 nm
m/e = 94
20°
1.0
0.5
0.0
N(t) (arb. units)
100
300
500
700
900
Flight time (μsec)

Fig. 9

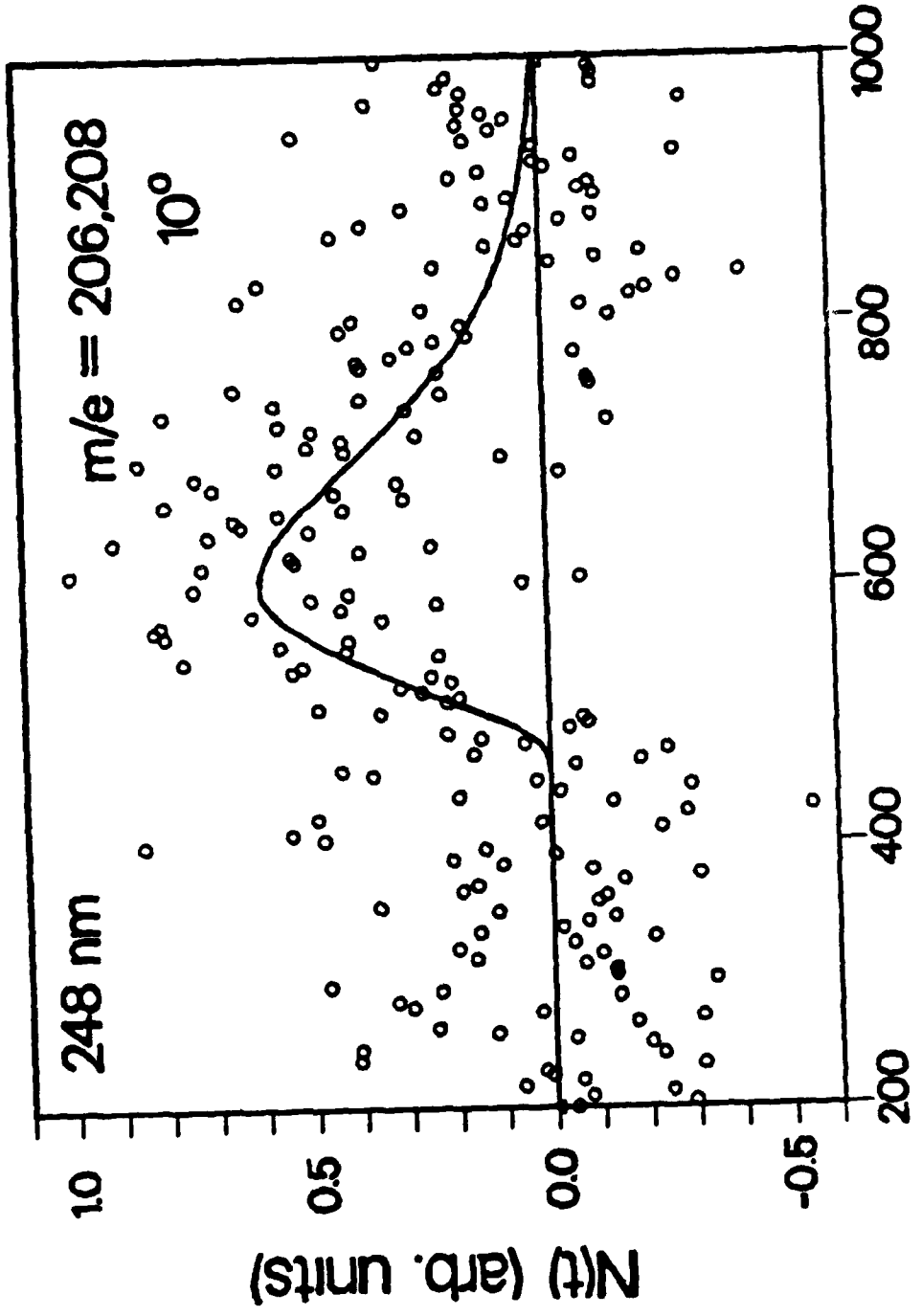
248 nm
m/e = 206,208
10°
N(t) (arb. units)
1.0
0.5
0.0
-0.5
200
400
600
800
1000
Flight time (μsec)

FIG. 10

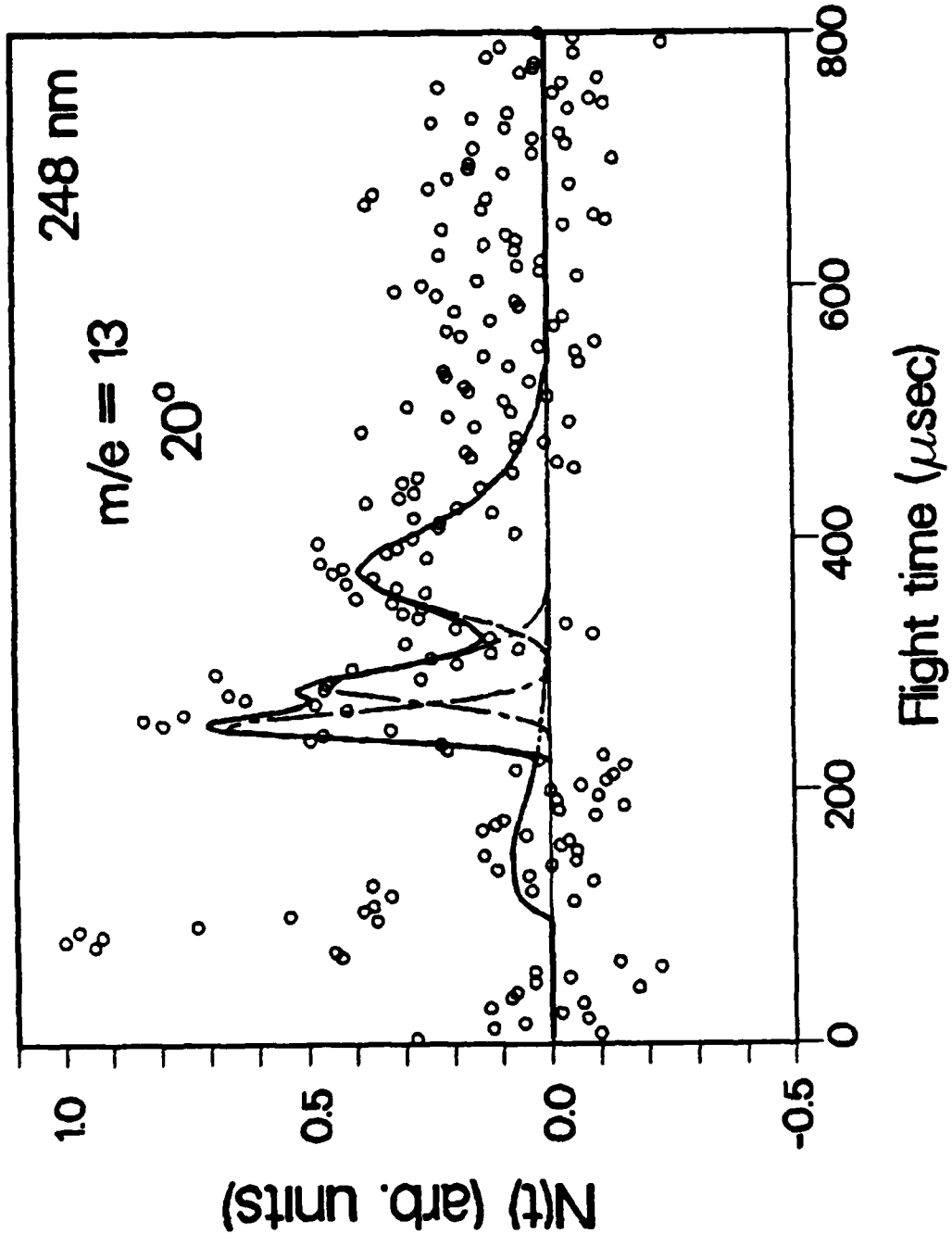
248 nm
m/e = 13
20°
N(t) (arb. units)
1.0
0.5
0.0
-0.5
0
200
400
600
800
Flight time (μsec)

Fig. 11

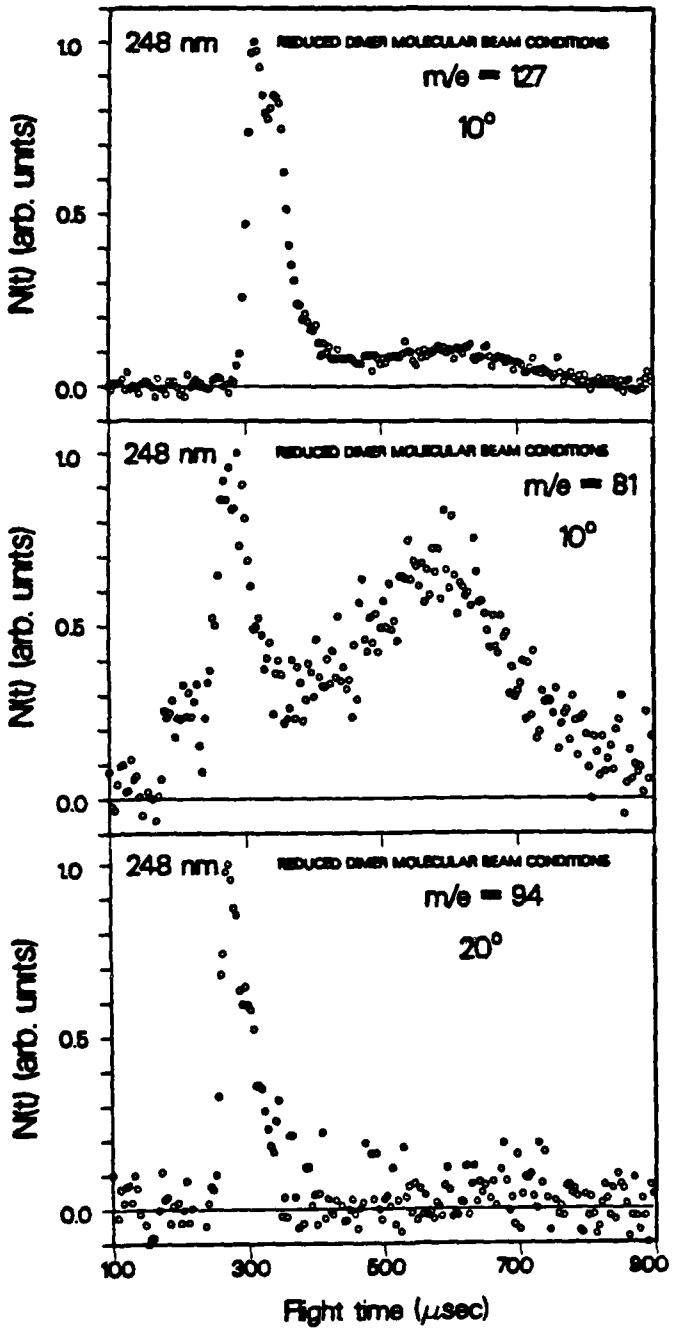
248 nm
REDUCED DIMER MOLECULAR BEAM CONDITIONS
m/e = 127
10°
N(t) (arb. units)
1.0
0.5
0.0
248 nm
REDUCED DIMER MOLECULAR BEAM CONDITIONS
m/e = 81
10°
N(t) (arb. units)
1.0
0.5
0.0
248 nm
REDUCED DIMER MOLECULAR BEAM CONDITIONS
m/e = 94
20°
N(t) (arb. units)
1.0
0.5
0.0
100
300
500
700
900
Flight time (μsec)

Fig. 12

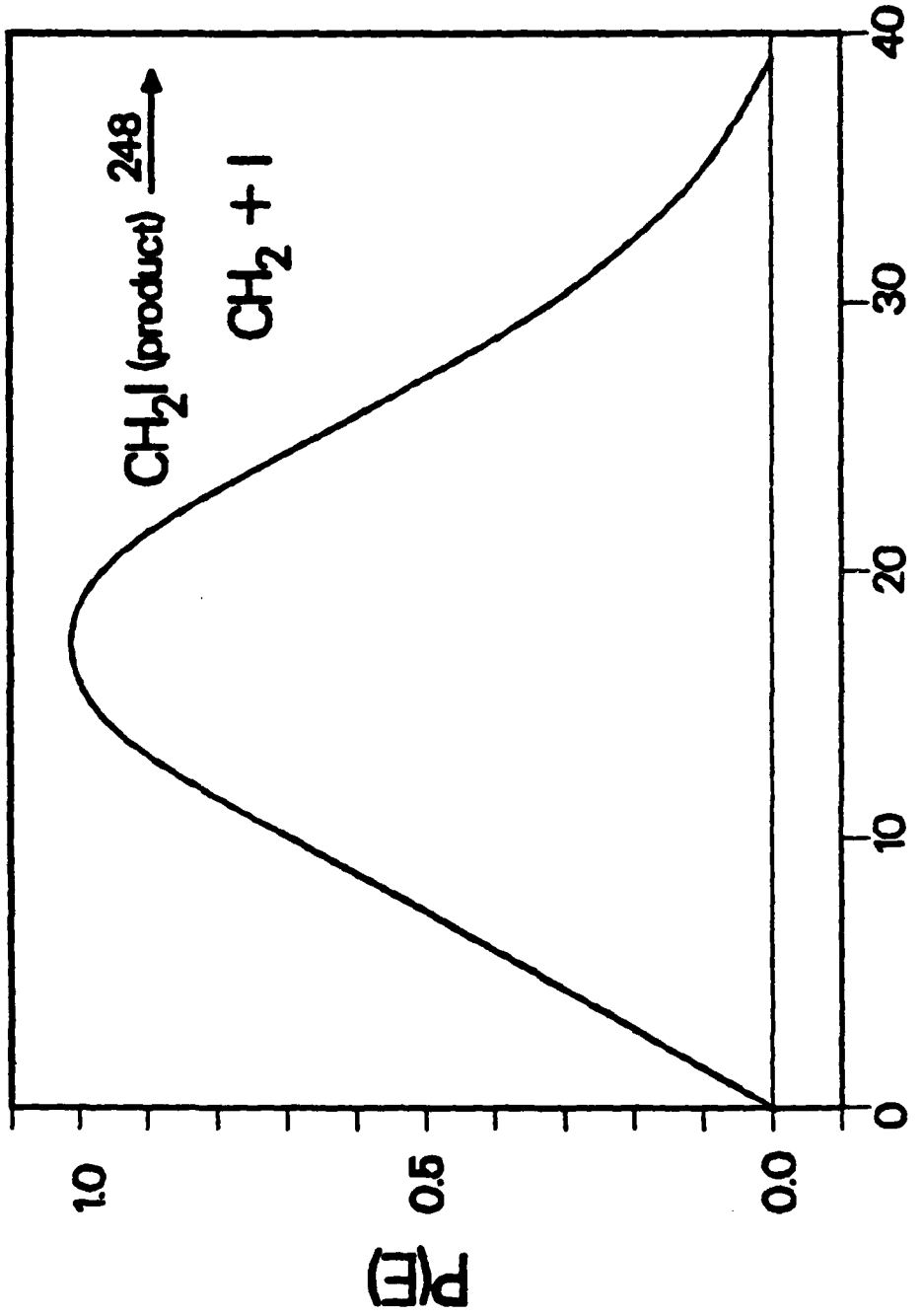

Fig. 13

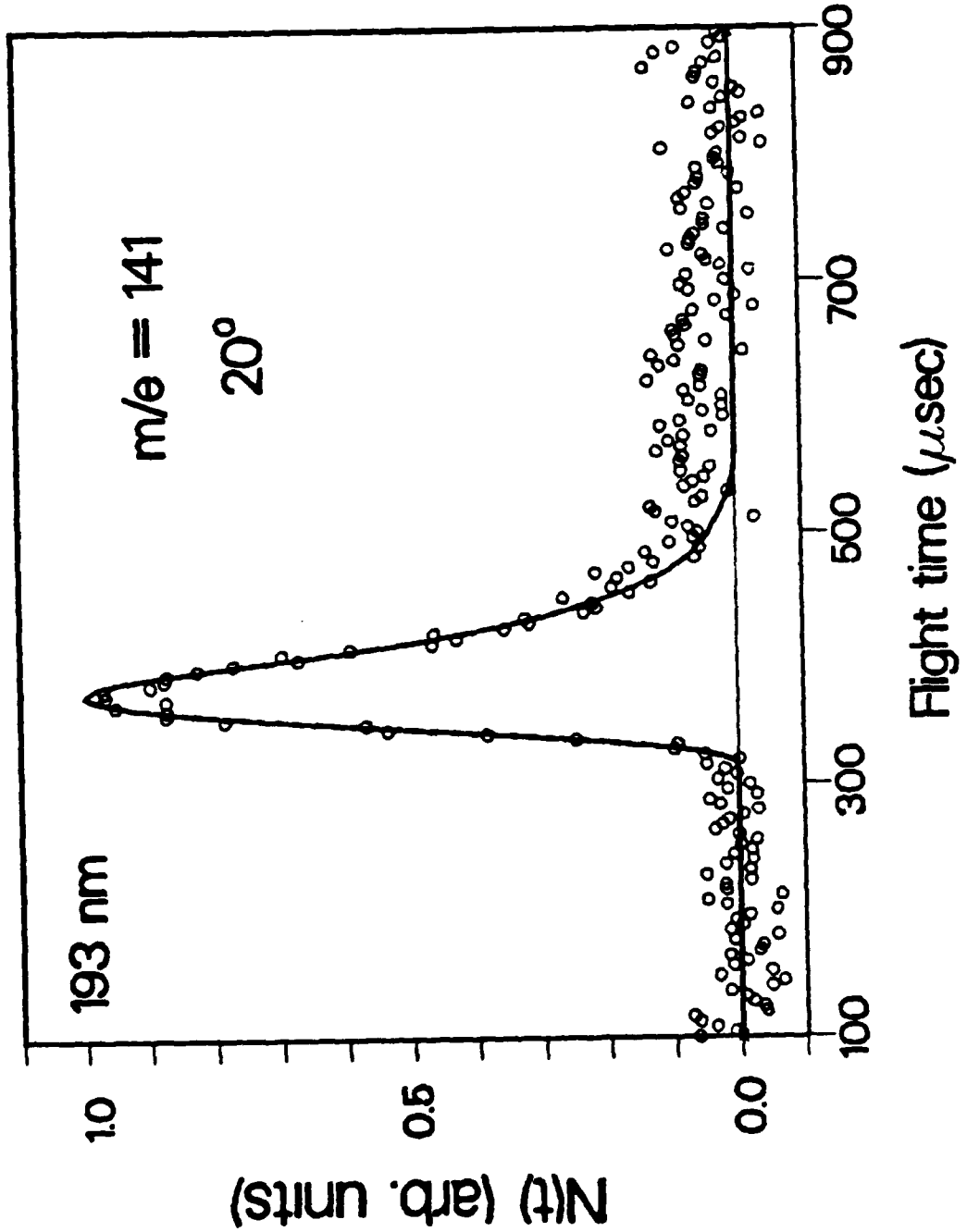
193 nm
m/e = 141
20°
N(t) (arb. units)
1.0
0.5
0.0
100
300
500
700
900
Flight time (μsec)

Fig. 14

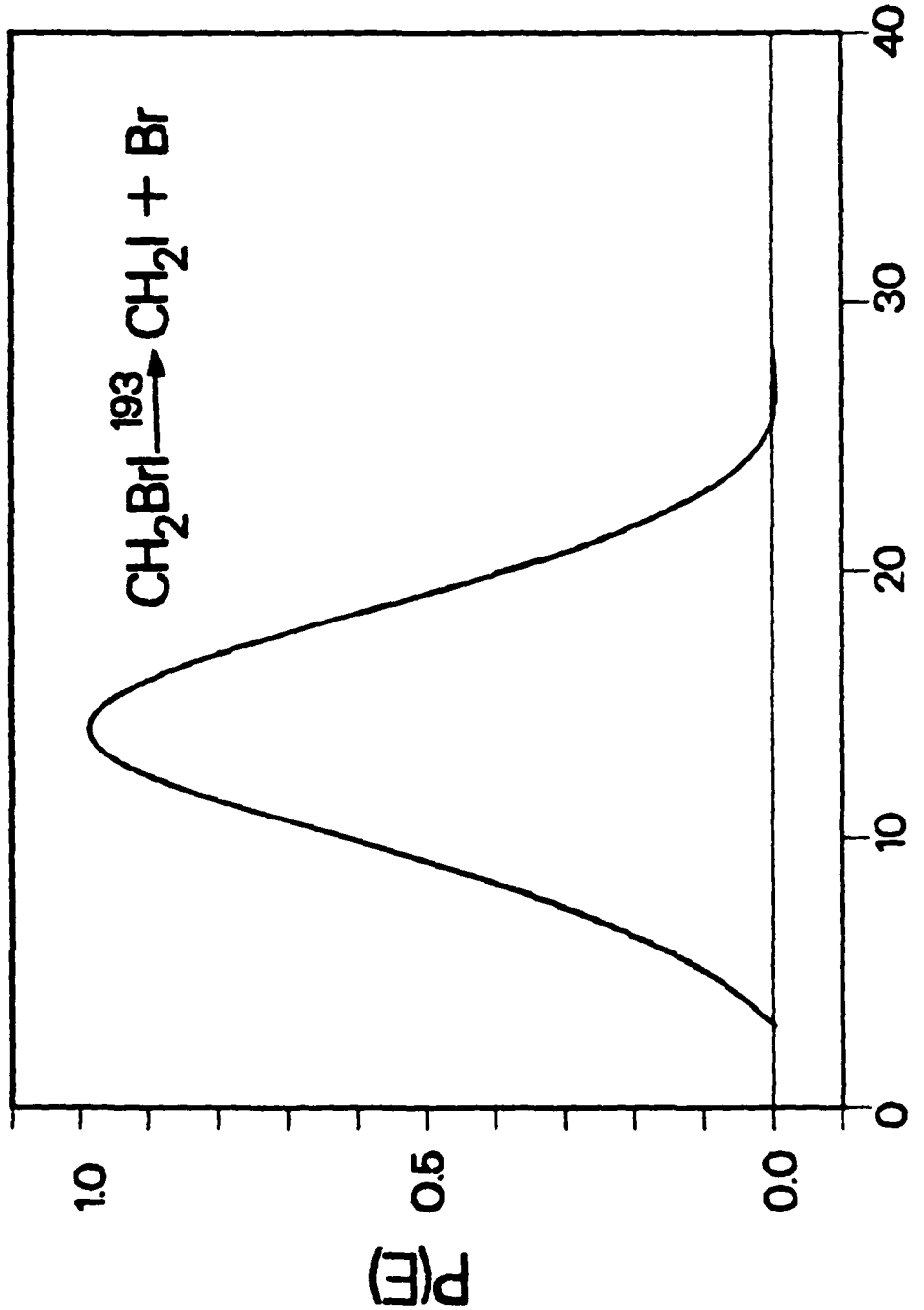
$CH_2BrI \xrightarrow{193} CH_2I + Br$
P(E)
1.0
0.5
0.0
0
10
20
30
40
ENERGY (kcal/mol)

Fig. 15

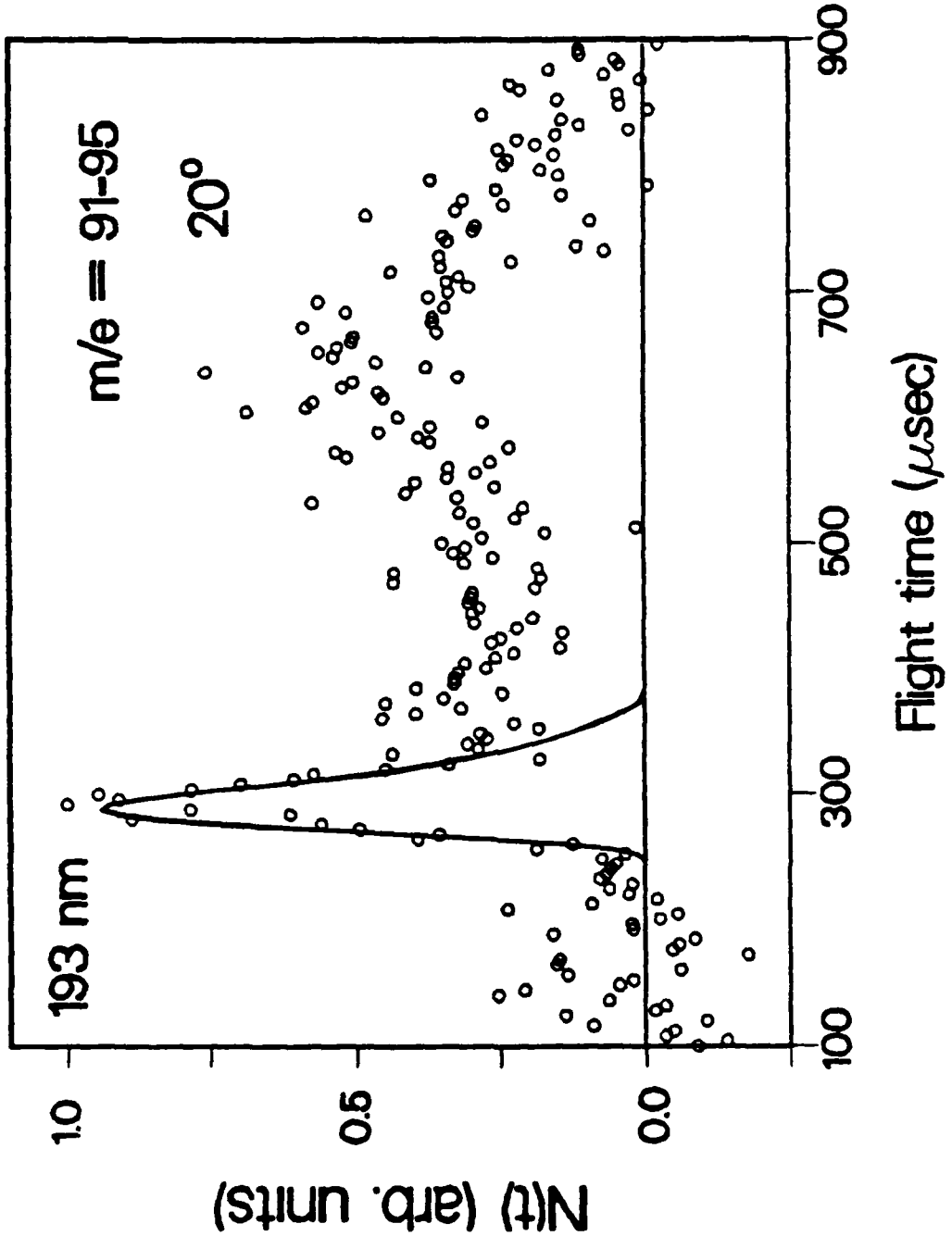
193 nm
m/e = 91-95
20°
N(t) (arb. units)
1.0
0.5
0.0
100
300
500
700
900
Flight time (μsec)

Fig. 16

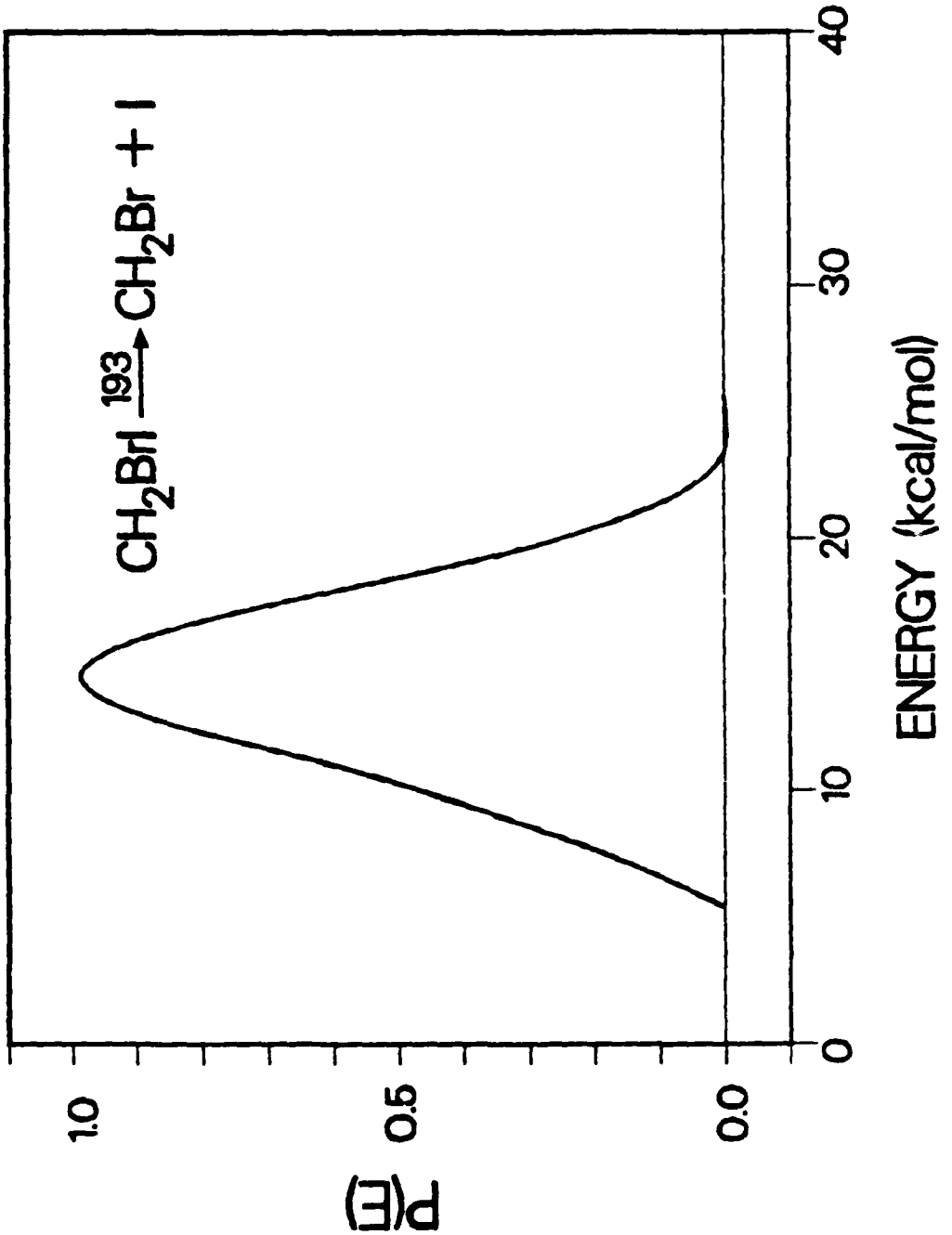
$CH_2BrI \xrightarrow{193} CH_2Br + I$
P(E)
1.0
0.5
0.0
0
10
20
30
40
ENERGY (kcal/mol)

Fig. 17

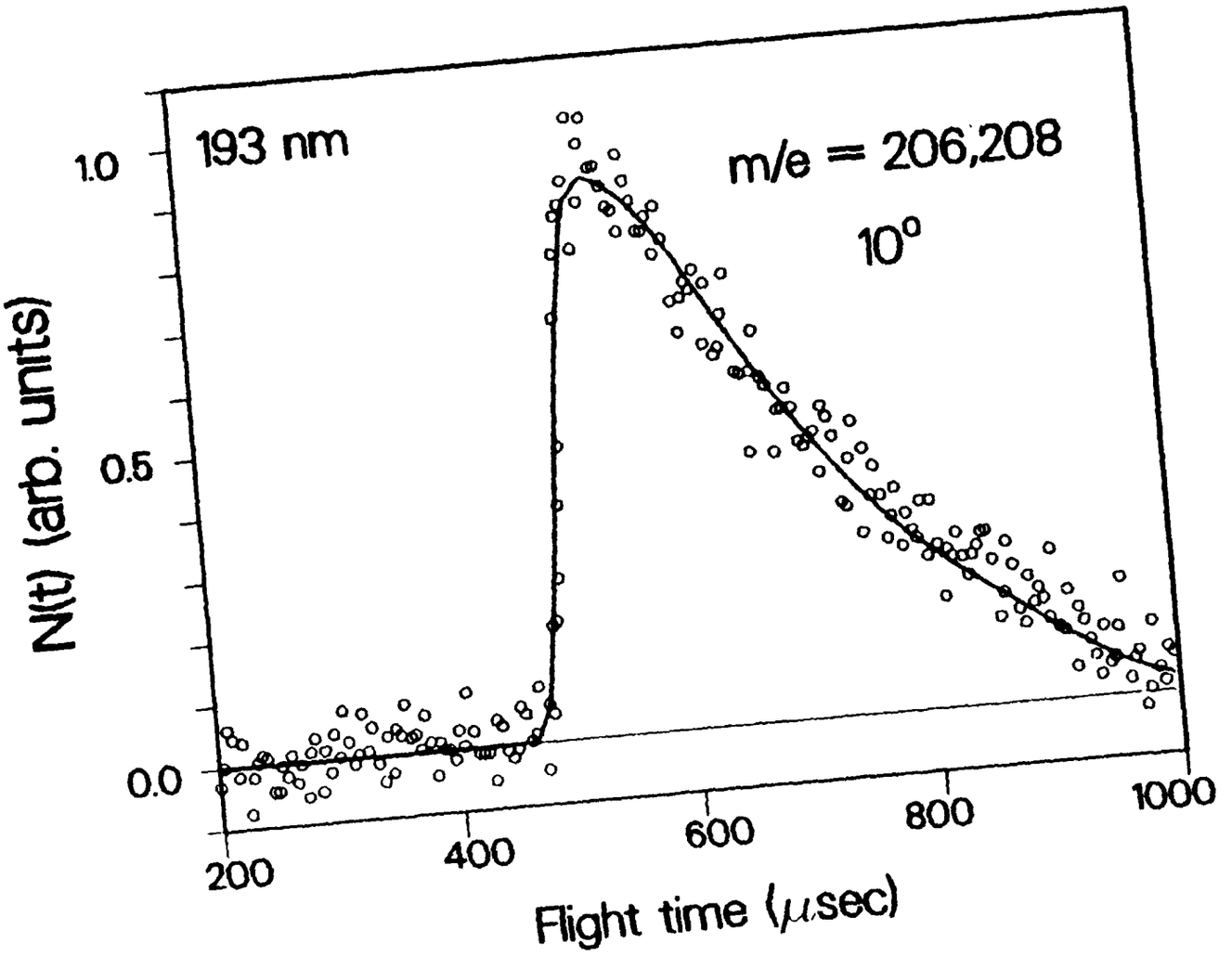
193 nm
m/e = 206,208
10°
1.0
0.5
0.0
N(t) (arb. units)
200
400
600
800
1000
Flight time (μsec)

Fig. 18

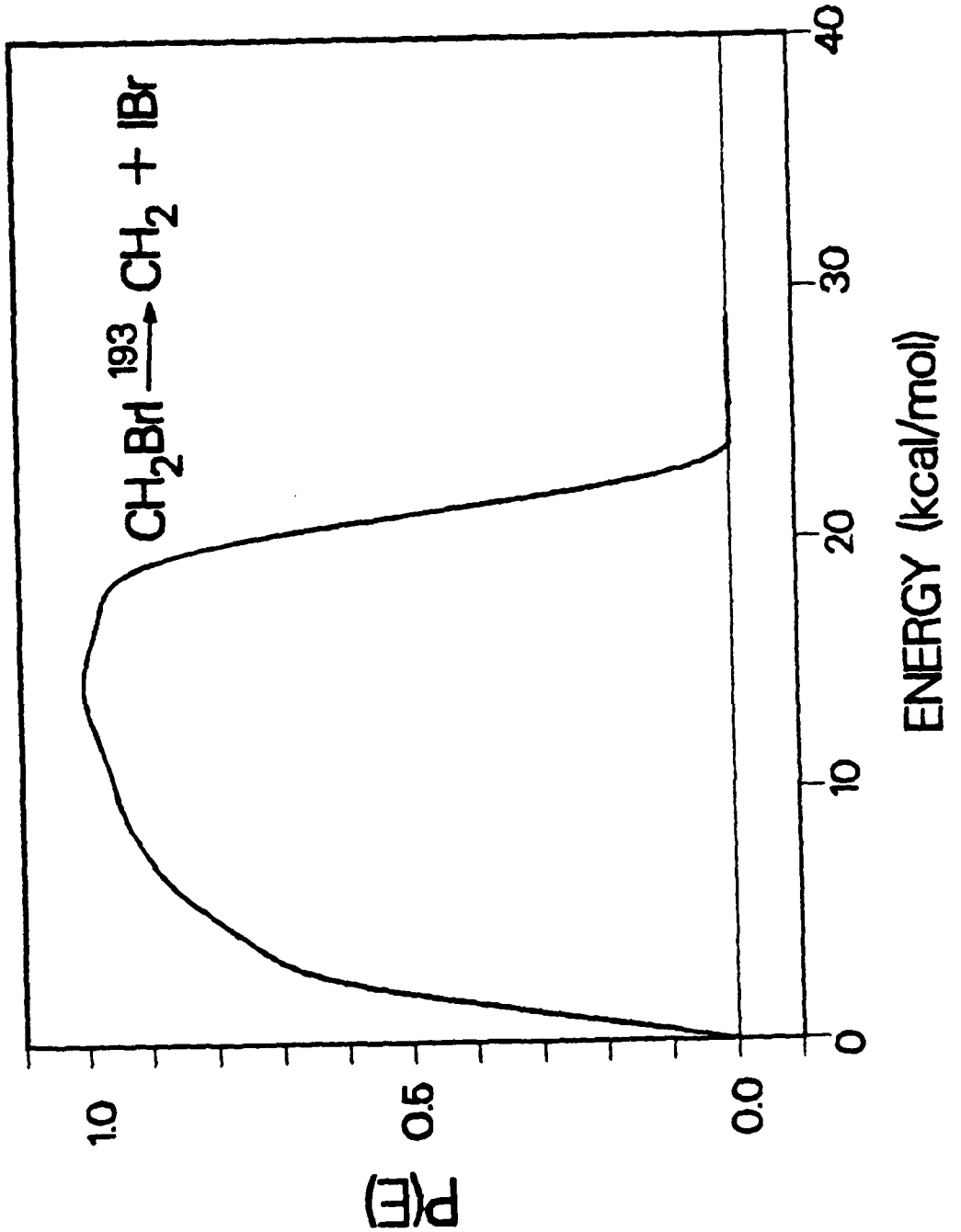
$CH_2BrI \xrightarrow{193} CH_2 + IBr$
P(E)
1.0
0.5
0.0
0
10
20
30
40
ENERGY (kcal/mol)

Fig. 19

END

FILMED

5-85

DTIC